The Evolution of Long-Period Comets

Paul Wiegert

Department of Physics and Astronomy, York University, Toronto, Ontario M3J 1P3, Canada
E-mail: wiegert@aries.phys.yorku.ca

and

Scott Tremaine

Princeton University Observatory, Peyton Hall, Princeton, New Jersey 08544-1001

We study the evolution of long-period comets by numerical integration of their orbits, a more realistic dynamical approach than the Monte Carlo and analytic methods previously used to study this problem. We follow the comets from their origin in the Oort cloud until their final escape or destruction, in a model solar system consisting of the Sun, the four giant planets and the Galactic tide. We also examine the effects of nongravitational forces as well as the gravitational forces from a hypothetical solar companion or circumsolar disk. We confirm the conclusion of Oort and other investigators that the observed distribution of long-period comet orbits does not match the expected steady-state distribution unless there is fading or some similar physical process that depletes the population of older comets. We investigate several simple fading laws. We can match the observed orbit distribution if the fraction of comets remaining observable after m apparitions is $\propto m^{-0.6\pm0.1}$ (close to the fading law originally proposed by Whipple 1962); or if approximately 95% of comets live for only a few ($\sim$6) returns and the remainder last indefinitely. Our results also yield statistics such as the expected perihelion distribution, distribution of aphelion directions, frequency of encounters with the giant planets and the rate of production of Halley-type comets. © 1999 Academic Press

Key Words: comets, dynamics; comets, origin; trans-neptunian objects.

1. INTRODUCTION

Comets can be classified on the basis of their orbital periods P into long-period (LP) comets with $P > 200$ yr and short-period (SP) comets with $P < 200$ yr. Short-period comets are further subdivided into Halley-type comets with 20 yr $< P < 200$ yr and Jupiter-family comets with $P < 20$ yr (Carusi and Valsecchi 1992). The boundary between SP and LP comets corresponds to a semimajor axis $a = (200)^{2/3}$ AU $= 34.2$ AU; this division is useful because (i) it distinguishes between comets whose aphelia lie within or close to the planetary system and those that venture beyond; (ii) an orbital period of 200 yr corresponds roughly to

the length of time over which routine telescopic observations have been taken—the sample of comets with longer periods is much less complete; (iii) the planetary perturbations suffered by comets with periods longer than 200 yr are uncorrelated on successive perihelion passages. The orbits of typical Halley-type and Jupiter-family comets are further distinguished by (i) their inclinations, which are much larger for Halley-type comets; (ii) their Tisserand invariants T, which are typically greater than 2 for Jupiter-family comets (Carusi and Valsecchi 1992; Levison 1996). In this paper we focus on the LP comets.

LP comets are believed to come from the Oort cloud (Oort 1950), a roughly spherical distribution of 10^{12}–10^{13} comets with semimajor axes between $10^{3.5}$ and 10^5 AU. The Oort cloud was probably formed from planetesimals ejected from the outer planetary region by planetary perturbations. LP comets—and perhaps some or all Halley-family comets—are Oort-cloud comets that have evolved into more tightly bound orbits under the influence of planetary and other perturbations (Fernández 1994; Weissman 1996a). Jupiter-family comets probably come from a quite different source, the Kuiper belt found just beyond Neptune.

The observed distributions of orbital elements of the $\sim$700 known LP comets are determined mainly by celestial mechanics, although physical evolution of the comets (e.g., fading or disruption during perihelion passage near the Sun) and observational selection effects (comets with large perihelion distances are undetectable) also play major roles. The aim of this paper is to construct models of the orbital evolution of LP comets and to compare these models to the observed distribution of orbital elements.

This problem was first examined by Oort (1950), who focused on the distribution of energy or inverse semimajor axis. He found that he could match the observed energy distribution satisfactorily, with two caveats: (i) he had to assume an *ad hoc* disruption probability $k = 0.014$ per perihelion passage; (ii) five times too many comets were present in a spike (the "Oort spike")

near zero energy. He argued that comets in the Oort spike, being typically on their first passage close to the Sun, may have a greater capacity for producing gaseous envelopes. This effect is now generally ascribed to the sublimation of volatile ices (e.g., CO, CO_2). When the comet subsequently returns (assuming it has avoided ejection and other loss mechanisms), the supply of volatiles has been depleted so the comet is fainter and hence may escape detection. Most of the decrease in brightness would occur during the first perihelion passage, and the brightness would level off as the most volatile components of the comet's inventory were lost. This "fading hypothesis" has played a central role in all subsequent attempts to compare the observed and predicted energy distributions of LP comets. The term "fading" will be generalized here to include *all* factors that reduce the intrinsic brightness of the comet near perihelion, and includes splitting into two or more large pieces, disruption into many small pieces, the depletion of volatiles, and the formation of insulating crusts of refractory materials.

In Section 2 we examine the observed distribution of LP comet orbits. The basic theoretical model of LP comet evolution is reviewed in Section 3. The simulation algorithm is described in Section 4, and the results are presented in Section 5. The simulations and results are described in more detail by Wiegert (1996).

2. OBSERVATIONS

The 1993 edition of the *Catalogue of Cometary Orbits* (Marsden and Williams 1993) lists 1392 apparitions of 855 individual comets, of which 681 are LP comets. Of these, 24 are considered to be members of the Kreutz group, believed to be fragments of a larger cometary body (Marsden 1967; Marsden 1989). The Kreutz group will be considered as a single comet here, reducing the sample to 658 LP comets. The Marsden–Williams catalog includes, where possible, the comet's osculating orbital elements at or near perihelion. When studying LP comets it is often simpler to work with the elements of the orbit on which the comet approached the planetary system, replacing the mass of the Sun by the mass of the Sun plus planets and working in the frame of the solar system barycenter (the "original" elements). These can be calculated from the orbit determined near perihelion by integrating the comet's trajectory backwards until it is outside the planetary system. Marsden and Williams list 289 LP comets that have been observed well enough (quality classes 1 and 2) so that reliable original elements can be computed. Three of these are Kreutz group objects, which we count as a single object, leaving a sample of 287.

The differences between the original elements and the elements near perihelion are generally small for the inclination[1] i, perihelion distance q, argument of perihelion ω, and longitude of the ascending node Ω; when examining the distribution of these elements we will therefore work with the entire sample ($N = 658$) of LP comets. The original semimajor axis and eccentricity are generally quite different from the values of these elements near perihelion, so when we examine these elements we will use only the smaller sample ($N = 287$) for which original elements are available.

2.1. Semimajor Axis

The energy per unit mass of a small body orbiting a point mass M is $-\frac{1}{2}GM/a$, where a is the semimajor axis.[2] For simplicity, we often use the inverse original semimajor axis $x \equiv 1/a$ as a measure of orbital energy (although this neglects the contribution to the energy from the Galactic potential, which can be important at large semimajor axes). The boundary between SP and LP comets is at $x = (200 \text{ yr})^{-2/3} = 0.029 \text{ AU}^{-1}$.

Figure 1 displays histograms of $x = 1/a$ for the 287 LP comets with known original orbits, at two different horizontal scales. The error bars on this and all other histograms are ± 1 standard deviation (σ) assuming Poisson statistics ($\sigma = N^{1/2}$), unless stated otherwise.

The sharp spike in the distribution for $x \lesssim 10^{-4} \text{ AU}^{-1}$ (the "Oort spike") was interpreted by Oort (1950) as evidence for a population of comets orbiting the Sun at large ($a \gtrsim 10\,000 \text{ AU}$) distances, a population which has come to be known as the Oort cloud. Comets in the spike are mostly dynamically "new" comets, on their first passage into the inner planetary system from the Oort cloud.

2.2. Perihelion Distance

Figure 2 shows the number of known LP comets versus perihelion distance q. The peak near 1 AU is due to observational bias: comets appear brighter when nearer both the Sun and the Earth. The intrinsic distribution $N(q)$, defined so that $N(q)\,dq$ is the number of detected *and* undetected LP comets with perihelion in the interval $[q, q + dq]$, is difficult to determine. Everhart (1967b) concluded that $N(q) \propto 0.4 + 0.6q$ for $q < 1$ AU, and that for $q > 1$ AU, $N(q)$ is poorly constrained, probably lying between a flat profile and one increasing linearly with q. Kresák and Pittich (1978) also found the intrinsic distribution of q to be largely indeterminate at $q > 1$ AU, but preferred a model in which $N(q) \propto q^{1/2}$ over the range $0 < q < 4$ AU. Shoemaker and Wolfe (1982) estimated $\int_0^q N(q)\,dq \propto 500q - 175$ for $q > 1.3$ AU.

These analyses also yield the completeness of the observed sample as a function of q. Everhart estimates that only 4% of observable comets with $q < 4$ AU are detected; the corresponding fraction in Shoemaker and Wolfe is 28%. Kresák and Pittich estimate that 60% of comets with $q \leq 1$ AU are detected, dropping to only 2% at $q = 4$ AU. Clearly the sample of LP comets is seriously incomplete beyond $q = 1$ AU, and the incompleteness

---

[1] Angular elements without subscripts are measured relative to the ecliptic. We shall also use elements measured relative to the Galactic plane, which we denote by a tilde, i.e., $\tilde{i}$, $\tilde{\Omega}$ and $\tilde{\omega}$.

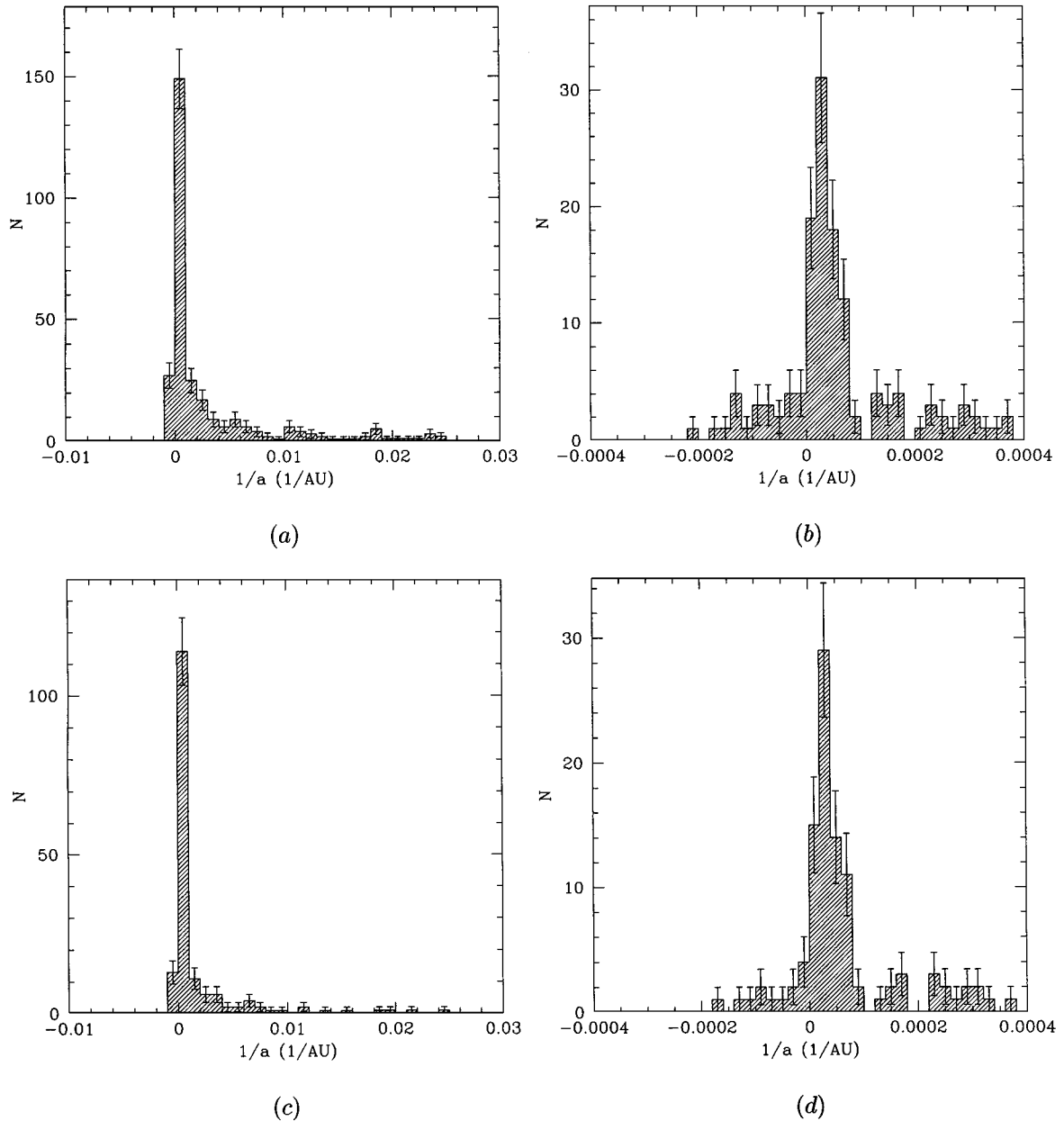[2] The units used in this paper when required are years, AU, and $M_\odot$, such that $G = 4\pi^2$.

FIG. 1. Distribution of original inverse semimajor axes of 287 LP comets at two different magnifications (panels *a,b*) and for the 170 LP comets with the most accurate Class I orbits (panels *c,d*). Data taken from Marsden and Williams (1993). There is no obvious difference between the top and bottom panels, suggesting that the inclusion of the less accurate Class II orbits does not severely distort the semimajor axis distribution.

is strongly dependent on q. In comparing the data to our simulations we must therefore impose a q-dependent selection function on our simulated LP comets. We shall generally do this in the crudest possible way, by declaring that our simulated comets are "visible" if and only if $q < q_v$, where q_v is taken to be 3 AU. This choice is unrealistically large—probably $q_v = 1.5$ AU would be better—but we find no evidence that other orbital elements are correlated with perihelion distance in the simulations, and the larger cutoff improves our statistics. We shall use the term "apparition" to denote a perihelion passage with $q < q_v$.

We have also explored a more elaborate model for selection effects based on work by Everhart (1967a,b; see Wiegert 1996 for details). In this model the probability p_v that an apparition is visible is given by

$$p_v(q) = \begin{cases} 0 & \text{if } q > 2.5 \text{ AU} \\ 2.5 - (q/1 \text{ AU}) & \text{if } 1.5 \leq q \leq 2.5 \text{ AU} \quad (1) \\ 1 & \text{if } q < 1.5 \text{ AU}. \end{cases}$$

The use of this visibility probability in our simulations makes very little difference in the distributions of orbital elements
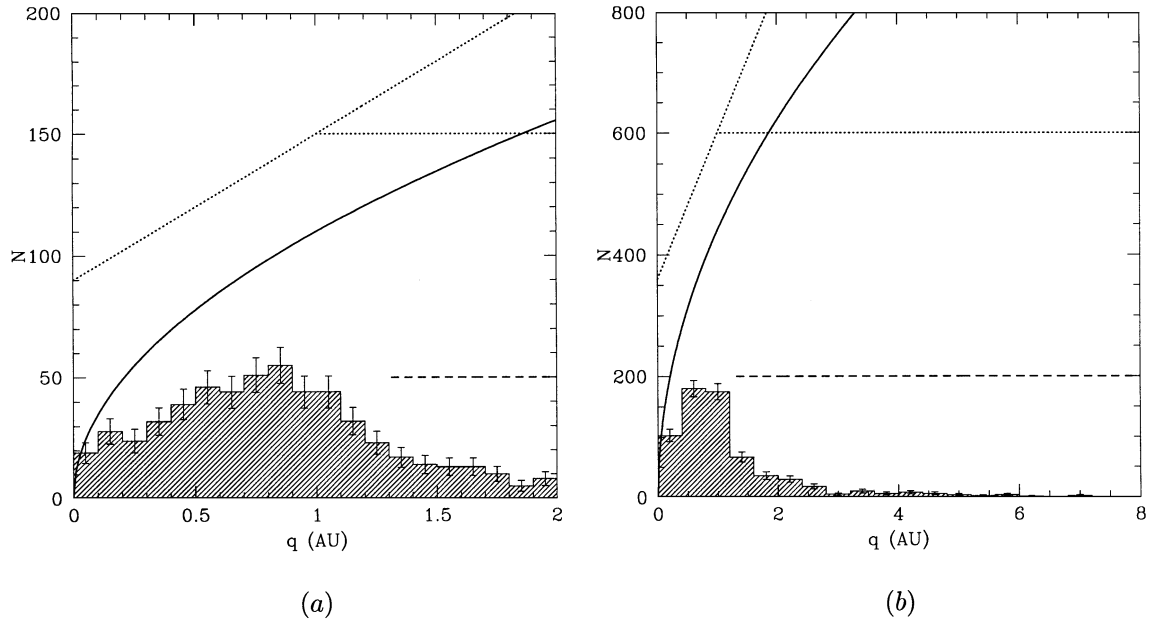
FIG. 2. Number N versus perihelion distance q for 658 LP comets, on two different horizontal scales. Data taken from Marsden and Williams (1993). The solid line is the estimated intrinsic distribution from Kresák and Pittich (1978), the two dotted lines are from Everhart (1967b), and the dashed line is from Shoemaker and Wolfe (1982). The appropriate normalizations are difficult to determine for the first two curves, and are chosen arbitrarily for plotting purposes.

(except, of course, for perihelion distance). For the sake of brevity we shall mostly discuss simulations using the simpler visibility criterion $q < q_v = 3$ AU.

2.3. Inclination

Figure 3 shows the distribution of the cosine of the inclination for the LP comets. A spherically symmetric distribution would be flat in this figure, as indicated by the heavy line. Everhart (1967b) argued that inclination-dependent selection effects affect this result at only the 10% level.

The inclination distribution in ecliptic coordinates is inconsistent with spherical symmetry: the χ^2 statistic indicates a low ($\lesssim 1\%$) probability that the distribution shown in Fig. 3a is flat (Nakamura 1979 and references therein). This is a result of the
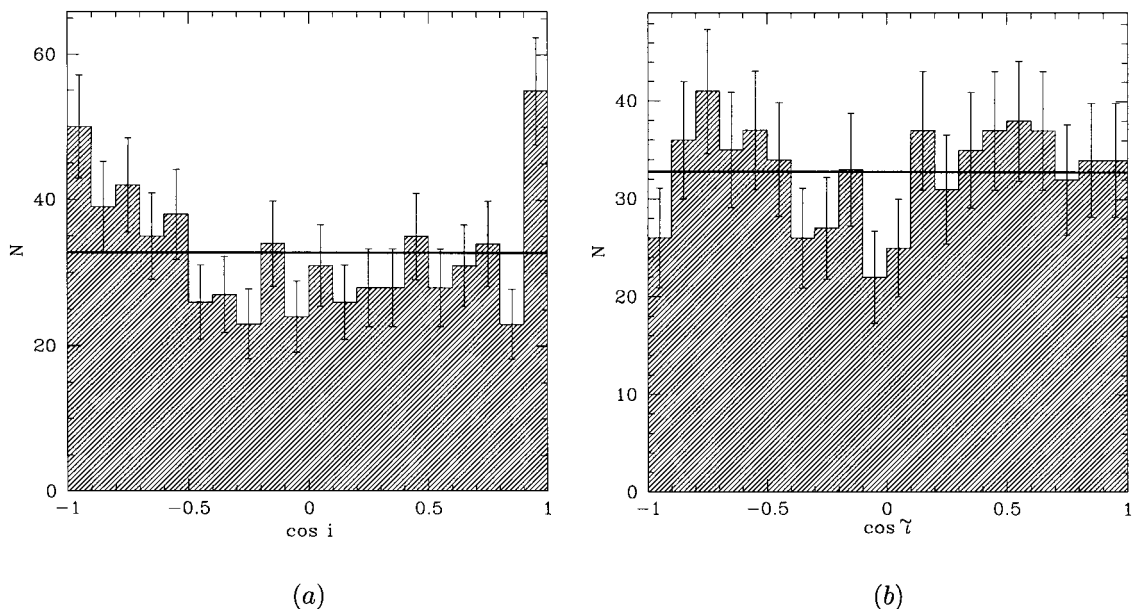

FIG. 3. The distribution of the cosine of the inclination for the 658 LP comets in (a) ecliptic coordinates, and (b) Galactic coordinates. A spherically symmetric distribution is indicated by the flat line. Data taken from Marsden and Williams (1993).
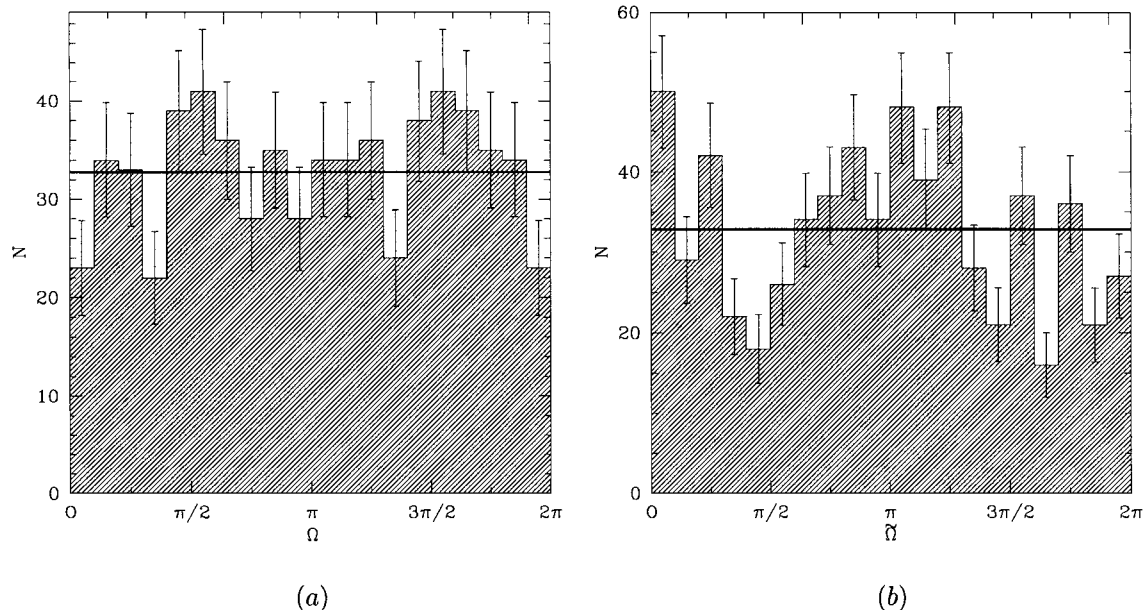
FIG. 4. The distribution of the longitude of the ascending node of the 658 LP comets in (a) ecliptic coordinates and (b) Galactic coordinates. Data taken from Marsden and Williams (1993).

excess of comets at $|\cos i| \sim 1$, possibly resulting from biases towards the ecliptic plane in comet searches and contamination by SP comets whose orbits are too poorly known to determine their eccentricity.

The inclination distribution in Galactic coordinates may have a gap near zero inclination, possibly reflecting the influence of the Galactic tide (4.1.2), or confusion from the dense background of stars and nebulae in the Galactic plane; however, the χ^2 statistic is consistent with a flat distribution at the 70% level. We will return to the features of this distribution in Section 2.6.

2.4. Longitude of Ascending Node

The distribution of longitude of the ascending node Ω is plotted in Fig. 4. The flat line again indicates a spherically symmetric distribution. Everhart (1967a, 1967b) concluded that Ω-dependent selection effects are likely to be negligible. The χ^2 test indicates that the ecliptic and galactic distributions are consistent with a flat distribution at only the 30% and $\lesssim 1\%$ levels, respectively.

2.5. Argument of Perihelion

Figure 5 shows the distribution of the argument of perihelion ω for the LP comets. Comets with $0 < \omega < \pi$ outnumber those with $\pi < \omega < 2\pi$ by a factor of $373/285 = 1.31 \pm 0.10$. This excess is probably due to observational selection (Everhart 1967a, Kresák 1982): comets with $0 < \omega < \pi$ pass perihelion north of the ecliptic, and are more easily visible to observers in the northern hemisphere. The distribution in the Galactic frame has an excess of comets with orbits in the range $\sin 2\tilde{\omega} > 0$ ($377/281 = 1.34 \pm 0.11$). This effect is almost certainly due to

the Galactic tide, which draws inward the perihelia of Oort-cloud comets with $\tilde{\omega}$ in this range (Section 4.3.2, Eq. (30)).

2.6. Aphelion Direction

Figure 6 shows the distribution of the aphelion directions of the LP comets in ecliptic and Galactic coordinates.

Claims have been made for a clustering of aphelion directions around the solar antapex (e.g., Tryor 1957; Oja 1975; Bogart and Noerdlinger 1982), but the presence of complex selection effects, such as the uneven coverage of the sky by comet searchers, renders difficult the task of unambiguously determining whether or not clustering is present. Newer analyses with improved catalogues (e.g., Lüst 1984; Neslusan 1996) have generally supported the hypothesis that LP aphelion directions are randomly distributed.

Whipple (1977) has shown that it is unlikely that there are many large comet groups (comets having split from the same parent body) in the observed sample though the numerous ($\sim$20) observed comet splittings makes the possibility acceptable in principle. A comet group would likely have spread somewhat in semimajor axis: the resulting much larger spread in orbital period $P \propto a^{3/2}$ makes it unlikely that two or more members of such a split group would have passed the Sun in the 200 yr for which good observational data exist. The Kreutz group of sun-grazing comets is the only generally accepted exception.

Figures 7a and b show histograms of comet number versus the sine of the ecliptic latitude β and of the Galactic latitude b of their aphelion directions. The ecliptic latitudes deviate only weakly from a spherically symmetric distribution and this deviation is likely due to the lack of southern hemisphere comet searchers. The Galactic distribution shows two broad peaks,
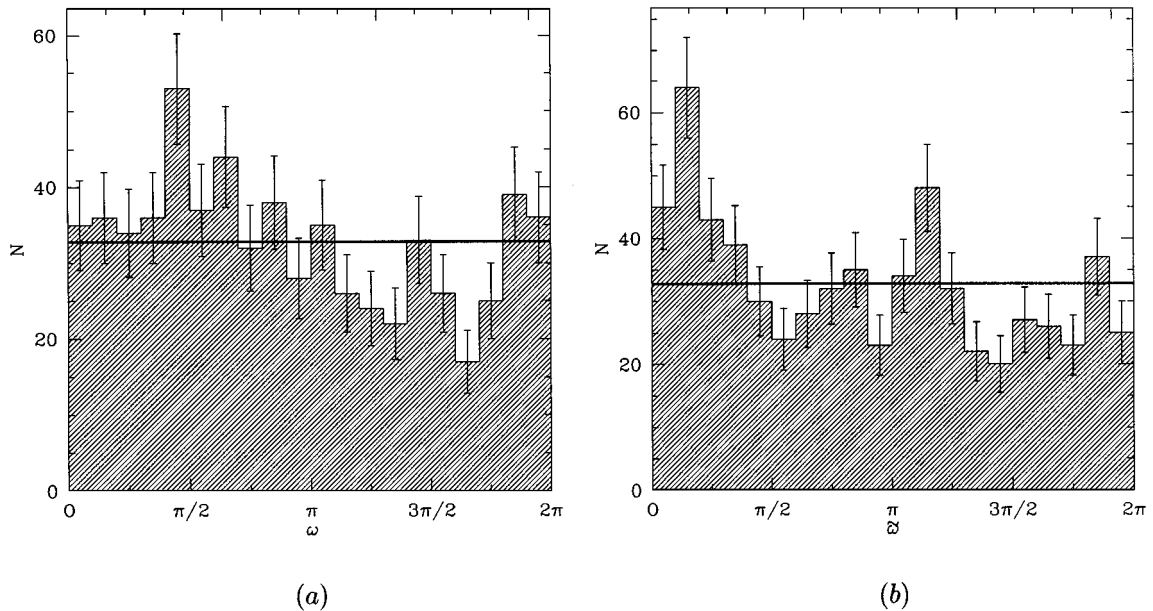
FIG. 5. The distribution of the argument of perihelion in (a) the ecliptic frame, ω, and (b) the Galactic frame, $\tilde{\omega}$, for the 658 LP comets. Data taken from Marsden and Williams (1993).

centered roughly on $\sin b \sim \pm 0.5$. It will be shown that these probably reflect the influence of the gravitational tidal field of the Galaxy, which acts most strongly when the Sun-comet line makes a $45°$ angle with the Galactic polar axis (Delsemme and Patmiou 1986).

2.7. Orbital Elements of Dynamically New Comets

For some purposes it is useful to isolate the distribution of orbital elements of the 109 dynamically new comets whose original semimajor axes lie in the Oort spike, $x = 1/a \leq 10^{-4}$ AU^{-1}. In particular, they will provide a basis of comparison with the dynamical models (Section 5.1). The distributions of perihelion distance, as well as inclination, longitude of the ascending node, and argument of perihelion in Galactic coordinates, are all shown in Fig. 8. The distribution of aphelion directions is shown in Fig. 9. We note again that the hyperbolic comets are included in these figures, on the assumption that they are coming from the Oort cloud.

2.8. Parameterization of the Distribution of Elements

For comparison with theoretical models, we shall parameterize the observed distribution of LP comets by three dimensionless numbers:

• The ratio of the number of comets in the Oort spike ($1/a < 10^{-4}$ AU^{-1}) to the total number of LP comets is denoted by Ψ_1. This parameter measures the relative strength of the Oort spike.
• The inverse semimajor axes of LP comets range from zero (unbound) to 0.029 AU^{-1} ($P = 200$ yr). Let the ratio of the number of comets in the inner half of this range (0.0145 to 0.029 AU^{-1}) to the total be Ψ_2. This parameter measures the prominence of the "tail" of the energy distribution.

• Let the ratio of the number of prograde comets in the ecliptic frame to the total be Ψ_3. This parameter measures the isotropy of the LP comet distribution.

We estimate these parameters using all LP comets with original orbits in Marsden and Williams (1993):

$$\Psi_1 = 109/287 = 0.380 \pm 0.043,$$
$$\Psi_2 = 19/287 = 0.066 \pm 0.015, \qquad (2)$$
$$\Psi_3 = 145/287 = 0.505 \pm 0.051.$$

For consistency, we based our calculation of Ψ_3 on the 287 comets with known original orbits, even though knowledge of the original orbit is not required since Ψ_3 depends only on angular elements. If we consider all 658 LP comets (again taking the Kreutz group to be a single comet), we find $\Psi_3 = 321/658 = 0.488 \pm 0.033$; the two values are consistent within their error bars.

We denote theoretical values of these parameters by Ψ_i^t and compare theory and observation through the parameters

$$X_i \equiv \frac{\Psi_i^t}{\Psi_i}, \quad i = 1, 2, 3, \qquad (3)$$

which should be unity if theory and observation agree.

3. THEORETICAL BACKGROUND

3.1. The Oort Cloud

The spatial distribution of comets in the Oort cloud can be deduced from the assumption that these comets formed in the outer planetary region and were scattered into the Oort cloud through the combined perturbations of the Galactic tide and
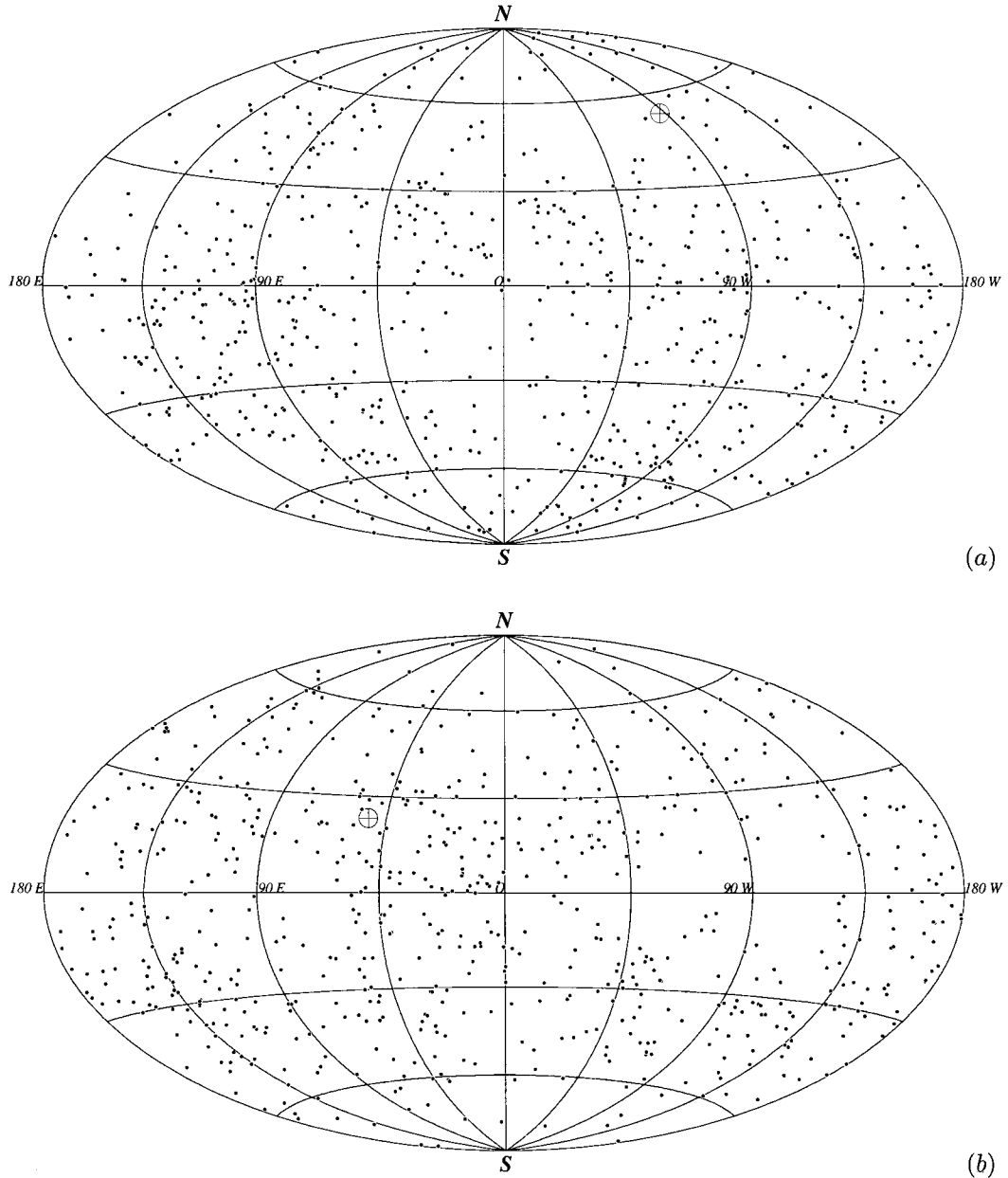
FIG. 6. All 658 long-period comet aphelion directions on ecliptic (a) and Galactic (b) equal-area maps. More precisely, these are the antipodes of the perihelion directions. The crossed circle is the solar apex. Data taken from Marsden and Williams (1993).

planets (Duncan *et al.* 1987). These calculations suggest—in order of decreasing reliability—that (i) the cloud is approximately spherical; (ii) the velocity distribution of comets within the cloud is isotropic; in other words the phase-space distribution is uniform on the energy hypersurface, except perhaps at very small angular momentum where the comets are removed by planetary encounters; (iii) the cloud's inner edge in semimajor axis is near 3000 AU, with a space number density of comets roughly proportional to $r^{-3.5}$ from 3000 to 50 000 AU.

Orbits of comets in the Oort cloud evolve mainly due to torques from the overall Galactic tidal field, but they are also affected by encounters with planets, passing stars and molecular clouds. Comets are also lost through collisions with the Sun and planets. Through these mechanisms, between 40% (Duncan *et al.* 1987) and 80% (Weissman 1985) of the original Oort cloud may have been lost over the lifetime of the Solar System, leaving perhaps 10^{12}–10^{13} comets (cf. Eq. (37)) with mass $\sim 40 M_{\oplus}$ (Weissman 1996a) in the present-day comet cloud. These numbers are uncertain by roughly an order of magnitude.

If the phase-space distribution of comets is uniform on the energy hypersurface, then the number of comets at a given semimajor axis with angular momentum less than J should be
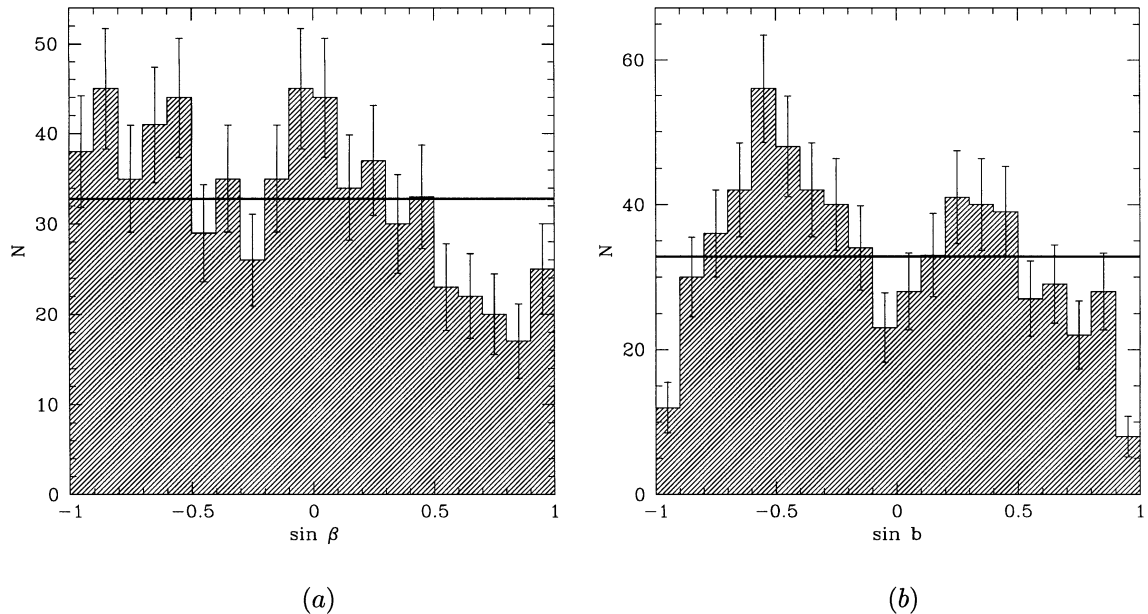
FIG. 7. The sine of the aphelion latitudes of the 658 LP comets in the ecliptic (a) and Galactic (b) reference frames. The heavy line indicates a spherically symmetric distribution. Data taken from Marsden and Williams (1993).

$\propto J^2$; this in turn implies that the number of comets with perihelion in the range $[q, q + dq]$ should be $N(q)\,dq$, where

$$N(q) \propto 1 - \frac{q}{a}, \quad q \le a \tag{4}$$

(Hills 1981). This distribution is modified if there are loss mechanisms that depend strongly on perihelion distance, as we now discuss.

3.2. The Loss Cylinder

A comet that passes through the planetary system receives a gravitational kick from the planets. The typical energy kick Δx depends strongly on perihelion distance (and less strongly on inclination): $\Delta x \approx 1 \times 10^{-3}$ AU^{-1} for $q \lesssim 6$ AU, dropping to 1×10^{-4} AU^{-1} at $q \simeq 10$ AU and 1×10^{-5} AU^{-1} at $q \simeq 20$ AU (van Woerkom 1948; Everhart 1968; Fernández 1981; Duncan *et al.* 1987). For comparison, a typical comet in the Oort spike has $x \lesssim 10^{-4}$ AU^{-1}. Since these comets have perihelion $q \sim 1$ AU, they receive an energy kick $\Delta x \gg x$ during passage through the planetary system. Depending on the sign of the kick, they will either leave the planetary system on an unbound orbit, never to return, or be thrown onto a more tightly bound orbit whose aphelion is much smaller than the size of the Oort cloud. In either case, the comet is lost from the Oort cloud. More precisely, only about 5% of dynamically new LP comets leave the planetary system with semimajor axes that again place them within the outer Oort cloud (Weissman 1978, 1979).

More generally, we can define a critical perihelion distance $q_l \sim 10$ AU such that comets with $q < q_l$ suffer a typical energy kick at perihelion which is larger than the typical energy in the

Oort cloud. Such comets are said to lie in the "loss cylinder" in phase space because they are lost from the Oort cloud within one orbit (the term "cylinder" is used because at a given location within the cloud, the constraint $q < q_l$ is satisfied in a cylindrical region in velocity space: for highly eccentric orbits $q < q_l$ implies that the angular momentum $J < J_l \equiv (2GM_\odot q_l)^{1/2}$, which in turn implies that the tangential velocity $v_\perp < J_l/r$). The loss cylinder is refilled by torques from the Galactic tide and other sources (*e.g.* Oort 1950; Weissman 1978; Hills 1981; Morris and Muller 1986; Torbett 1986).

The comets in the Oort spike are inside the loss cylinder and hence must generally be on their first passage through the planetary system (this is why we designated the 109 comets with $1/a < 10^{-4}$ AU^{-1} as dynamically "new" in Section 2.7). The loss cylinder concept also explains why the energy spread in the Oort spike is much narrower than the energy spread in the Oort cloud itself: comets with smaller semimajor axes have a smaller moment arm and shorter period so their per-orbit angular momentum and perihelion distance changes are smaller; for $a \lesssim 2 \times 10^4$ AU the perihelion cannot jump the "Jupiter barrier," *i.e.*, cannot evolve from $q > q_l \sim 10$ AU (large enough to be outside the loss cylinder) to $q \lesssim 1$ AU (small enough to be visible) in one orbital period (Weissman 1985). Thus the inner edge of the Oort spike is set by the condition that the typical change in angular momentum per orbit equals the size of the loss cylinder, and does not reflect the actual size of the Oort cloud (Hills 1981). The new comets we see come from an outer or active Oort cloud ($a \gtrsim 2 \times 10^4$ AU) in which the typical change in angular momentum per orbit exceeds the radius of the loss cylinder. Thus, in the outermost regions of the Oort cloud, losses from planetary perturbations do not strongly
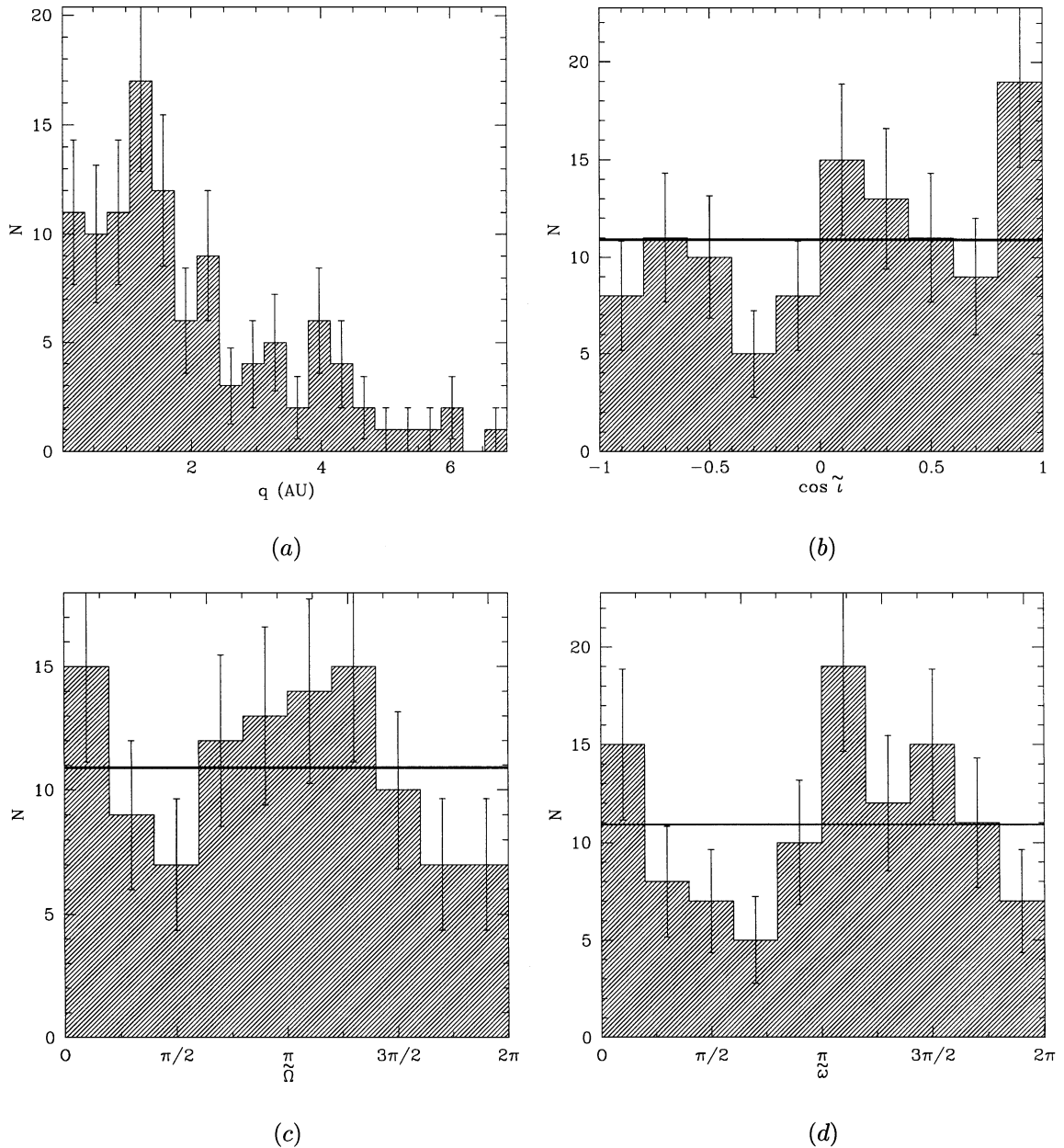
FIG. 8.   Distribution of orbital elements for the 109 dynamically new comets ($1/a < 10^{-4}$ AU^{-1}): (a) perihelion distance; (b) inclination; (c) longitude of ascending node; (d) argument of perihelion. All angular elements are measured in the Galactic frame.

affect the phase-space distribution of comets near zero angular momentum (the loss cylinder is said to be "full"), and the equilibrium distribution of perihelion distances (Eq. (4)) remains approximately valid within the loss cylinder. The more massive inner Oort cloud ($a \lesssim 2 \times 10^4$ AU) does not produce visible comets except during a rare comet "shower" caused by an unusually close stellar encounter which perturbs them sufficiently to jump the Jupiter barrier (Hills 1981; Bailey *et al.* 1987; Fernández and Ip 1987; Heisler *et al.* 1987; Hut *et al.* 1987; Heisler 1990; Whipple 1994). In this inner cloud, losses from planetary perturbations strongly deplete the distribution

of comets at small perihelion distances (the loss cylinder is said to be "empty") and thus it does not contribute to the Oort spike.

3.3. Energy Evolution of LP Comets

Let us examine the motion of an Oort-cloud comet after it enters the planetary system for the first time. The motion of a comet in the field of the giant planets, the Sun, and the Galactic tide is quite complicated, but considerable analytic insight can be obtained if we approximate the comet's evolution after it enters the loss cylinder as a random walk in energy, with the
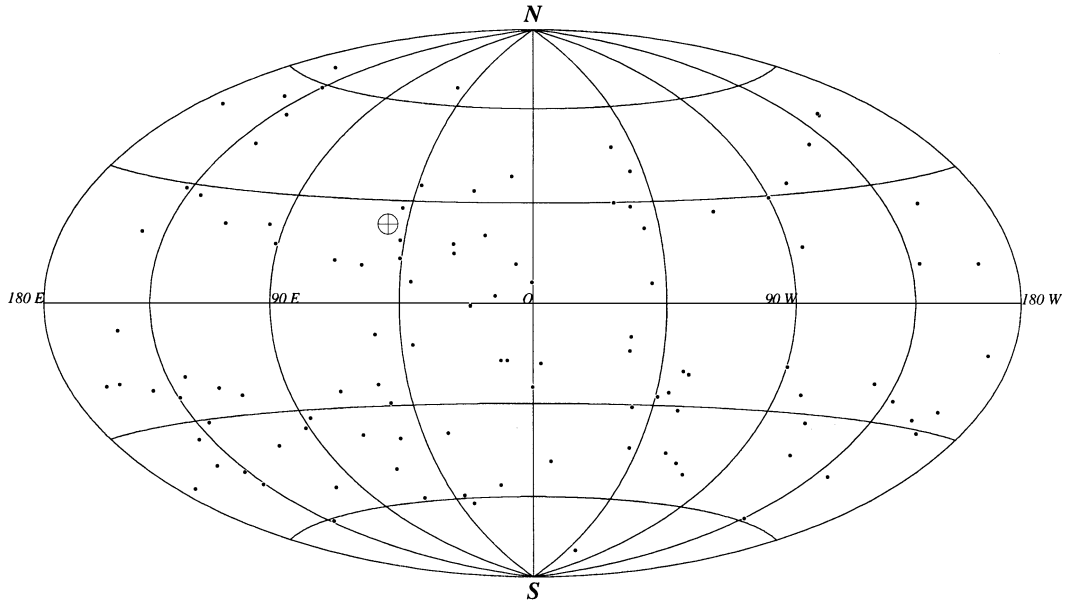
FIG. 9. Equal-area plot of the aphelion directions of the 109 dynamically new comets in the Galactic frame. The crossed circle is the solar apex.

other orbital elements remaining constant. The energy kicks occur near the comet's perihelion passage, the only phase of the orbit at which planetary perturbations are important (planetary perturbations also affect the comet's other orbital elements, but to a much smaller relative degree since the energy is small when the semimajor axis is large). The random walk continues until the comet reaches an unbound orbit ($x \leq 0$) or some arbitrary inner barrier, usually taken to be the LP–SP boundary. The assumption that comets disappear when they become SP comets is unrealistic, but our simulations show that the fraction of LP comets that survive fading and ejection to become SP comets is small enough that the details of SP comet evolution are unlikely to affect the distribution of LP comets.

These simplifying assumptions have formed the basis of analyses by many authors (*e.g.* Oort 1950; Kendall 1961; Whipple 1962; Lyttleton and Hammersley 1963; Weissman 1978). The random-walk approximation can be justified for comets with large semimajor axes using simple dynamical models based on area-preserving maps (Petrosky 1986; Sagdeev and Zaslavsky 1987; Chirikov and Vecheslavov 1989).

Recall that the term "fading" is used here to denote any change in the properties of the comet that would cause it to disappear from the observed sample. We parametrize the fading process by a function $\Phi_m \in [0, 1]$, $m = 1, 2, \ldots$ ($\Phi_1 = 1$), the probability that a visible, dynamically new comet survives fading for at least m perihelion passages. There are two closely related functions: the probability that the comet will survive for precisely m perihelion passages,

$$\phi_m \equiv \Phi_m - \Phi_{m+1}, \qquad (5)$$

and the conditional probability that a comet that survives m

passages will fade before the $(m + 1)$st passage,

$$\psi_m = \frac{\phi_m}{\Phi_m} = 1 - \frac{\Phi_{m+1}}{\Phi_m}. \qquad (6)$$

The simplest version of the random-walk problem is obtained by assuming that there is no fading ($\psi_m = 0$) and that the energy changes by discrete steps $\pm\epsilon$ with equal probability. In this case the possible values of the energy are restricted to a lattice $x = (j - 1)\epsilon$, where j is an integer, and the random walk is identical to the gambler's ruin problem (Kannan 1979; Feller 1968). The end-state of ejection ($j = 0$) corresponds to bankruptcy; if in addition we assume that there is an absorbing boundary at $x_{sp} \equiv (j_{sp} - 1)\epsilon$, then evolving to an SP comet corresponds to breaking the house. Thus, for example, the probabilities that an LP comet with energy $(j - 1)\epsilon$ will eventually be ejected or become a short-period comet are respectively

$$p_{ej} = 1 - \frac{j}{j_{sp}}, \quad p_{sp} = \frac{j}{j_{sp}}, \qquad (7)$$

and the mean number of orbits that the comet will survive is

$$\langle m \rangle = j(j_{sp} - j). \qquad (8)$$

A new comet has $j = 1$ and its mean lifetime is therefore $\langle m \rangle = j_{sp} - 1$; the ratio of new to all LP comets observed in a fixed time interval is

$$\Psi_1^t = \frac{1}{\langle m \rangle} = \frac{1}{j_{sp} - 1}. \qquad (9)$$

There are also explicit expressions for the probability that the

comet is ejected or becomes an SP comet at the mth perihelion passage (Feller 1968).

The gambler's ruin problem is particularly simple if there is no boundary condition at large x ($x_{sp} \to \infty$), which is reasonable since few comets reach short-period orbits anyway (Section 5.2.1). The probability that a new comet will be ejected on the mth orbit is then

$$p_{ej}(m) = \frac{1}{2^m m} \binom{m}{\frac{1}{2}m + \frac{1}{2}}, \quad m \text{ odd}, \tag{10}$$
$$= 0, \qquad\qquad m \text{ even};$$

for $m \gg 1$, $p_{ej}(m) \to (2/\pi)^{1/2} m^{-3/2}$ for m odd, and zero otherwise. The mean lifetime $\sum_{m=1}^{\infty} m p_{ej}(m)$ is infinite. The probability that a comet will survive for at least m orbits is $\sim m^{-1/2}$ for large m; this agrees with the empirical results of Everhart (1976) and Weissman (1978).

When using the gambler's ruin to model the evolution of LP comets, we take $\epsilon \simeq 5 \times 10^{-4}$ AU^{-1}, which is the RMS energy change for comets with perihelion between 5 and 10 AU (Fernández 1981; Duncan *et al.* 1987) and $x_{sp} = 0.029$ AU^{-1} ($P = 200$ yr); thus $j_{sp} \simeq 60$. Equation (9) then predicts $\Psi_1^t = 0.017$; the ratio of the predicted to the observed value for this parameter (cf. Eq. (3)) is

$$X_1 = \frac{\Psi_1^t}{\Psi_1} = 0.051 \pm 0.006. \tag{11}$$

The gambler's ruin model predicts far too few comets in the Oort spike relative to the total number of LP comets.

This simple model also makes useful predictions about the inclination distribution of LP comets. The distribution of dynamically new comets is approximately isotropic, so there are equal numbers of prograde and retrograde new comets. Since prograde comets have longer encounter times with the planets, they tend to have larger energy changes than retrograde comets. Equation (9) predicts that the ratio of prograde to retrograde LP comets should be roughly the ratio of the RMS energy change for these two types, $\epsilon_{retro}/\epsilon_{pro} \simeq 2$–$3$. The fraction of prograde comets should then be $\Psi_3^t = 1/(1 + \epsilon_{pro}/\epsilon_{retro}) \simeq 0.3$. The ratio of the predicted to the observed value for this parameter (cf. Eq. (3)) is

$$X_3 = \frac{\Psi_3^t}{\Psi_3} = 0.58 \pm 0.06. \tag{12}$$

The gambler's ruin model predicts too few prograde comets.

More accurate investigations of this one-dimensional random walk have been carried out by many authors since 1950. Although the observational data have improved dramatically over this interval, the results from comparing the data to theoretical models have remained remarkably consistent.

Oort (1950) approximated the probability distribution of energy changes $p(\Delta x)$ by a Gaussian and assumed $\psi_m = k = $ cons-

tant. He found a good fit to most of the energy distribution for $k = 0.014$; however, he found that the number of new comets was larger than the model predicted by a factor of 5, and hence was forced to assume that only one in five new comets survive as visible comets to their second perihelion passage—in other words $\psi_1 = 0.8$, $\psi_m = 0.014$ for $m > 1$. Kendall (1961) and Yabushita (1979) have analyzed the case $x_{sp} \to \infty$, $\psi_m = k = $ constant, $p(y) \propto \exp(-2^{1/2}|y|/\sigma)$, where σ is the RMS energy change per perihelion passage. Kendall derives a reasonable fit to the data if $k = 0.04$ and one in four to six new comets survive to the second perihelion—results roughly compatible with Oort's. Kendall's model predicts a ratio of new comets to all LP comets observed in a fixed time interval given by $\Psi_1^t = k^{1/2} = 0.2$. Yabushita (1979) gave analytic formulae for $p_{ej}(m)$ for this model, and showed that the probability that a comet will survive for at least m orbits is $\sim \exp(-km)/m^{1/2}$ for large m. Whipple (1962) examined survival laws of the form $\phi_m \propto m^{-\alpha}$ (the proportionality constant is determined by the condition that $\sum_m \phi_m = 1$) and found a good fit to the observed energy distribution with $\alpha \simeq 1.7$. Everhart (1979) used a distribution $p(y)$ derived from his numerical experiments and found $\Phi_m \simeq 0.2$ for all $m > 1$; in other words only one in five comets survived to the second perihelion passage but the fading after that time was negligible.

For some purposes the random walk can be approximated as a diffusion process; in this case the relevant equations and their solutions are discussed by Yabushita (1980). Bailey (1984) examines solutions of a diffusion equation in two dimensions (energy and angular momentum) and includes a fading probability that depends on energy rather than perihelion number—which is less well motivated but makes the equations easier to solve (he justifies his fading function with an *a posteriori* "thermal shock" model, in which comets with large aphelia are more susceptible to disruption because they approach perihelion with a lower temperature). Bailey finds a good fit to the observed energy distribution if the fading probability per orbit is

$$\phi(x) = 0.3\left[1 + (x/0.004 \text{ AU})^2\right]^{-3/2}. \tag{13}$$

Emel'yanenko and Bailey (1996) have modeled the distribution of LP comets using a Monte Carlo model with $\psi_m = k = $ constant plus an additional probability per orbit k^* that the comet is rejuvenated. Their preferred values are $k = 0.3$ and $k^* = 0.0005$.

The most complete model of LP comet evolution based on a random walk in energy is due to Weissman (1978, 1979, 1980). His Monte Carlo model included the gravitational influence of the planets, nongravitational forces, forces from passing stars, tidal disruption by and/or collision with the Sun and planets, and fading and splitting. In his preferred model, 15% of the comets have zero disruption probability, and the rest had a probability of 0.1 per orbit; using these assumptions, Weissman was able to successfully reproduce the semimajor axis, inclination, and perihelion distributions.

The one-dimensional random walk is a valuable tool for understanding the distribution of LP comets. However, some of its

assumptions are not well justified: (i) Secular changes in perihelion distance, argument of perihelion, and inclination at each perihelion passage accumulate over many orbits and can lead to substantial evolution of the orientation and perihelion (Quinn *et al.* 1990; Bailey *et al.* 1962; Thomas and Morbidelli 1996). (ii) Although the probability distribution of energy changes $p(y)$ is approximately an even function [$\langle y^2 \rangle^{1/2}$ is larger than $\langle y \rangle$ by $O(M_p/M_\odot)$], the random changes in energy due to the second moment grow only as $m^{1/2}$ where m is the number of orbits, while the systematic changes due to the first moment grow as m. Thus the small asymmetry in $p(y)$ may have important consequences. (iii) The approximation that successive changes in energy are uncorrelated neglects possible resonances between the comet and planetary orbital periods.

For example, a number of other investigations have found significant discrepancies between the predictions of the one-dimensional random walk or diffusion approximation and more accurate techniques. Dones *et al.* (1996) found that the diffusion approximation overestimated the median lifetime of Centaurs by a factor ranging from 1 to 10. Duncan and Levison (1997) found that 1% of Neptune-crossing test particles survived for the age of the solar system, a fraction far larger than the diffusion approximation predicts (most of the survivors were trapped in resonant orbits). Similarly, Malyshkin and Tremaine (1998) found that the long-term survival of planet-crossing orbits in the planar restricted three-body problem was much larger than predicted by the diffusion approximation, a result they attribute to resonance sticking.

3.4. The Fading Problem

All the investigations described in the previous subsection reach the same conclusion: if the LP comets are in a steady state then one or more mechanisms ("fading") must remove most, or at least some, of the comets from our observed sample after their first perihelion passage (Oort 1950; Whipple 1962; Marsden and Sekanina 1973). Therefore either (i) the comet distribution is not in a steady state, which almost certainly requires rejecting most of the Oort model,[3] or (ii) we must postulate *ad hoc* fading laws and abandon the use of the energy distribution as a convincing test of the Oort model. This is the fading problem.

Fading can arise from many possible mechanisms but the most natural hypothesis is that the comet's brightness fades sharply because its near-surface inventory of ices more volatile than water is depleted during the first perihelion passage. Oort and Schmidt (1951) have argued that this hypothesis is supported by the observation that dynamically new comets have strong continuum spectra due to dust entrained by the gases from a volatile

component, and that the decline of brightness with increasing heliocentric distance is much slower for new comets. Many authors have looked for evidence that new comets differ in composition or brightness from older LP comets, with mixed results; Whipple (1991) summarizes these investigations by saying that the Oort–Schmidt effect is "fairly well confirmed."

Fading is much slower after the first perihelion passage, as exemplified by the long history of Halley's comet. Whipple (1992) concludes that there is no strong evidence that older (i.e., shorter period) LP comets have faded relative to younger LP comets, consistent with theoretical estimates that 10^3–10^4 orbits are required for moderate-sized comets to lose their volatiles (Weissman 1980) and the lack of strong systematic trends in the brightness of SP comets (e.g., P/Halley, Stephenson *et al.* 1985).

Comets may also fade if they disrupt or split. After splitting, the fragments may be fainter and hence less likely to be visible, and in addition lose their volatiles more rapidly. Moreover, young comets are more likely to split than old ones: Weissman (1980) gives splitting probabilities per perihelion passage of 0.10 ± 0.04 for dynamically new comets but only 0.045 ± 0.011 for LP comets in general. The cause of splitting is not well understood, except in some cases where splitting is due to tidal forces from a close encounter with the Sun or a giant planet.

Finally, we note that LP comets are responsible for 10–30% of the crater production by impact on Earth (Shoemaker 1983; Weissman 1990). The observed cratering rate can therefore—in principle—constrain the total population of LP comets, whether or not they have faded; however, this constraint is difficult to evaluate, in part because estimates of comet masses are quite uncertain.

4. ALGORITHM

We represent each comet by a massless test particle and neglect interactions between comets. The orbit of the test particle is followed in the combined gravitational fields of the Sun, the four giant planets, and the Galactic tide. We assume that the planets travel around the Sun in circular, coplanar orbits. We neglect the terrestrial planets, Pluto, the small free inclinations and eccentricities of the giant planets, and their mutual perturbations, as there is no reason to expect that these play significant roles in the evolution of LP comets.

4.1. Equations of Motion

The equations of motion of the comet can be written as

$$\ddot{\mathbf{r}} = \mathbf{F}_\odot + \mathbf{F}_{\text{planets}} + \mathbf{F}_{\text{tide}} + \mathbf{F}_{\text{other}}, \qquad (14)$$

where the terms on the right side represent the force per unit mass from the Sun, the planets, the Galactic tide, and other sources (e.g., nongravitational forces).

4.1.1. The planets. We shall employ two frames of reference: the barycentric frame, whose origin is the center of mass of the Sun and the four planets, and the heliocentric frame, whose

---

[3] There are advocates of this position (see Bailey 1984 for references), but we are not among them. It is possible that we are currently in a comet shower; however (i) the duty cycle of showers is only about 2% (Heisler 1990, Weissman 1996a,b), so the *a priori* probability that we are in a shower is small; (ii) the prominent Oort spike seen in the observations would be erased during a shower except near the beginning of the shower.

origin is the Sun. In the barycentric frame,

$$\mathbf{F}_\odot + \mathbf{F}_{\text{planets}} = -\frac{GM_\odot}{|\mathbf{r} - \mathbf{r}_\odot|^3}(\mathbf{r} - \mathbf{r}_\odot) - \sum_p \frac{GM_p}{|\mathbf{r} - \mathbf{r}_p|^3}(\mathbf{r} - \mathbf{r}_p), \tag{15}$$

where $\mathbf{r}$, $\mathbf{r}_\odot$, and $\mathbf{r}_p$ are the positions of the comet, the Sun, and planet p. In the heliocentric frame, the Sun is at the origin and

$$\mathbf{F}_\odot + \mathbf{F}_{\text{planets}} = -\frac{GM_\odot}{|\mathbf{r}|^3}\mathbf{r} - \sum_p \frac{GM_p}{|\mathbf{r} - \mathbf{r}_p|^3}(\mathbf{r} - \mathbf{r}_p)$$
$$- \sum_p \frac{GM_p}{|\mathbf{r}_p|^3}\mathbf{r}_p; \tag{16}$$

the last sum is the "indirect term" that arises because the heliocentric frame is not inertial.

The heliocentric frame is useful for integrating orbits at small radii, $|\mathbf{r}| \lesssim |\mathbf{r}_p|$, because it ensures that the primary force center, the Sun, is precisely at the origin (see Section 4.1.4). It is not well suited for integrating orbits at large radii, $|\mathbf{r}| \gtrsim |\mathbf{r}_p|$, because the indirect term does not approach zero, and it oscillates with a period equal to the planetary orbital period—thereby forcing the integrator to use a very small time step. In the integrations we switch from heliocentric to barycentric coordinates when the comet radius $|\mathbf{r}|$ exceeds a transition radius r_c; tests show that the integrations are most efficient when $r_c = 10$ AU.

The code tracks close encounters and collisions between comets and planets. A close encounter with a planet is defined to be a passage through a planet's sphere of influence

$$R_I = \left(\frac{M_p}{M_\odot}\right)^{2/5} a_p, \tag{17}$$

where a_p is the planet's semimajor axis. Each inward crossing of the sphere of influence is counted as one encounter, even if there are multiple pericenter passages while the comet remains within the sphere of influence. A close encounter with the Sun is defined to be a passage within 10 solar radii.

4.1.2. The Galactic tide. The effects of the Galactic tide on comet orbits are discussed by Antonov and Todriya (1984), Heisler and Tremaine (1986), Morris and Muller (1986), Torbett (1986), and Matese and Whitman (1989). Consider a rotating set of orthonormal vectors $\{\mathbf{e}_{\tilde{x}}, \mathbf{e}_{\tilde{y}}, \mathbf{e}_{\tilde{z}}\}$. Let $\mathbf{e}_{\tilde{x}}$ point away from the Galactic center, $\mathbf{e}_{\tilde{y}}$ in the direction of Galactic rotation, and $\mathbf{e}_{\tilde{z}}$ towards the South Galactic Pole (South is chosen so that the coordinate system is right-handed). The force per unit mass from the tide is (Heisler and Tremaine 1986)

$$\mathbf{F}_{\text{tide}} = (A - B)(3A + B)\tilde{x}\mathbf{e}_{\tilde{x}} - (A - B)^2\tilde{y}\mathbf{e}_{\tilde{y}}$$
$$- \left[4\pi G\rho_0 - 2(B^2 - A^2)\right]\tilde{z}\mathbf{e}_{\tilde{z}}, \tag{18}$$

where ρ_0 is the mass density in the solar neighborhood, and A and B are the Oort constants. We take $A = 14.4 \pm 1.2$ km s^{-1} kpc^{-1} and $B = -12.0 \pm 2.8$ km s^{-1} kpc^{-1} (Kerr and Lynden-Bell 1986).

The local mass density is less well known. Visible matter (stars and gas) contributes about 0.1 M$_\odot$ pc^{-3}, but the amount of dark matter present in the solar neighborhood remains controversial. If the dark matter is distributed like the visible matter, then the dark/visible mass ratio P is between 0 and 2 (Oort 1960; Bahcall 1984; Kuijken and Gilmore 1989; Kuijken 1991; Bahcall *et al.* 1992). We adopt $\rho_0 = 0.15$ M$_\odot$ pc^{-3} in this paper, corresponding to $P = 0.5$.

With these values of A, B, and ρ_0, the $4\pi G\rho_0$ term of Eq. (18) exceeds the others by more than a factor of 10, and from now on we shall neglect these other terms. The dominant component of the tidal force arises from a gravitational potential of the form

$$V_{\text{tide}} = 2\pi G\rho_0 \tilde{z}^2. \tag{19}$$

In practice, of course, the local density ρ_0 varies as the Sun travels up and down, in and out, and through spiral arms during its orbit around the Galaxy. The amplitude of this variation depends strongly on the unknown distribution and total amount of disk dark matter. The maximum-to-minimum density variation could be as large as 3:1 (Matese *et al.* 1995) but is probably considerably smaller, with a period around 30 Myr [close to $\frac{1}{2}(\pi/G\rho_0)^{1/2}$, the half-period for oscillations in the potential (19)]. We are justified in neglecting these variations in ρ_0, because the typical lifetime of LP comets after their first apparition is only 1.4 Myr (see Table 3), which is much shorter.

4.1.3. Encounters with stars and molecular clouds. Our model neglects the effects of passing stars on LP comets, for three main reasons: (i) The delivery rate of Oort-cloud comets to the planetary system due to Galactic tides is higher than the rate due to stellar encounters by a factor of 1.5–2 (Heisler and Tremaine 1986; Torbett 1986), except during rare comet showers caused by an unusually close passage, during which the delivery rate may be enhanced by a factor of 20 or so (Hills 1981; Heisler 1990). We feel justified in neglecting the possibility of a comet shower for the reasons given in footnote 3 above. (ii) The effects of stellar encounters are highly time-variable whereas the strength of the tide is approximately constant over the typical lifetime of LP comets; thus by concentrating on the effects of the tide we focus on a deterministic problem, whose results are easier to interpret. (iii) The evolution of LP comets after their entrance into the planetary system is dominated by interactions with the planets, the tide and passing stars playing little role—and matching the evolved, rather than the injected, comet distribution is the main challenge of the fading problem.

We also neglect encounters with molecular clouds, since the effects of these rare encounters are difficult to estimate reliably because the properties of molecular clouds are poorly known (Bailey 1983; Drapatz and Zinnecker 1984; Hut and Tremaine 1985; Torbett 1986).

4.1.4. Regularization. Integrating the orbits of LP comets is a challenging numerical problem, because of the wide range of time scales (the orbital period can be several Myr but

perihelion passage occurs over a time scale of a few years to a few months) and because it is important to avoid any secular drift in energy or angular momentum due to numerical errors. We have used the Kustaanheimo–Stiefel (K–S) transformation to convert Cartesian coordinates to regularized coordinates and have carried out all of our integrations in the regularized coordinates. A requirement of K–S regularization is that the frame origin must coincide with the primary force center, which is why we use heliocentric coordinates at small radii.

The numerical integrations were carried out using the Bulirsch–Stoer method, which was checked using a fourth-order Runge–Kutta–Fehlberg algorithm. All integrations were done in double-precision arithmetic.

4.2. Nongravitational Forces

The asymmetric sublimation of cometary volatiles results in a net acceleration of the nucleus. These nongravitational[4] (NG) forces are limited to times of significant outgassing (*i.e.*, coma production), and remain small even then.

Nongravitational forces are difficult to model. Their strength obviously depends on the comet's distance from the Sun, but displays less regular variability as well: gas production may vary by a factor of 2 or more between the pre- and postperihelion legs of the orbit (Sekanina 1964; Festou 1986), and jets and streamers are observed to evolve on time scales of less than a day (Festou *et al.* 1993b), suggesting that NG forces change on similar time scales. Further complications arise from the rotation of the nucleus, which is difficult to measure through the coma, and which may be complicated by precession (Wilhelm 1987).

The NG acceleration $\mathbf{F}_{\text{jet}}$ is written as

$$\mathbf{F}_{\text{jet}} = F_1\mathbf{e}_1 + F_2\mathbf{e}_2 + F_3\mathbf{e}_3, \qquad (20)$$

where $\mathbf{e}_1$ points radially outward from the Sun, $\mathbf{e}_2$ lies in the orbital plane, pointing in the direction of orbital motion and normal to $\mathbf{e}_1$, and $\mathbf{e}_3 = \mathbf{e}_1 \times \mathbf{e}_2$. A naive model of NG accelerations, which is all the data allow, assumes that the short time-scale components are uncorrelated and cancel out, leaving only fairly regular, longer time-scale components as dynamically important. We shall use the Style II model of Marsden *et al.* (1973), which assumes that accelerations are symmetric about perihelion, and can be represented by

$$F_1(r) = A_1 g(r), \quad F_2(r) = A_2 g(r), \quad F_3(r) = A_3 g(r). \qquad (21)$$

Here $\{A_1, A_2, A_3\}$ are independent constants, and $g(r)$ is a non-negative function describing the dependence on the comet–Sun

distance r. The form of $g(r)$ is based on an empirical fit to a theoretical water sublimation curve by Delsemma and Miller (1971),

$$g(r) = C\left(\frac{r}{r_0}\right)^{-m}\left[1 + \left(\frac{r}{r_0}\right)^n\right]^{-k}, \qquad (22)$$

where $m = 2.15$, $k = 4.6142$, $n = 5.093$, $r_0 = 2.808$ AU, and C is chosen to be 0.1113 so that $g(1 \text{ AU}) = 1$. Note that $g(r)$ is roughly proportional to $r^{-m} \approx r^{-2}$ for $r \ll r_0$. At $r \gg r_0$, $g(r)$ decreases much faster than the simple inverse square that describes the incident solar flux.

The constants A_i are determined by fitting individual comet orbits (Mersden *et al.* 1973); the value of A_1 is typically 10^{-7} to 10^{-9} AU day^{-2}, $|A_2|$ is typically only 10% of $|A_1|$, and A_3 is consistent with zero. A_1 is generally well determined for all comets, but A_2 is often indeterminate for LP comets.

4.3. Initial Conditions

4.3.1. Initial phase-space distribution. The distribution of comets in the Oort cloud is only poorly known, although it is plausible to assume that the cloud is roughly spherical and that the comets are uniformly distributed on the energy hypersurface in phase space, except possibly at very small angular momenta (cf. Section 3.1). Then the phase-space density f is a function only of $L \equiv (GM_\odot a)^{1/2}$, which we assume to be

$$f(L) = \begin{cases} 0, & L < L_- = (GM_\odot a_-)^{1/2}, \\ f_0 L^{2\alpha+3}, & L_- \leq L \leq L_+, \\ 0, & L > L_+ = (GM_\odot a_+)^{1/2}, \end{cases} \qquad (23)$$

where f_0 and α are constants, and a_- and a_+ are the semimajor axes of the inner and outer edges of the Oort cloud, respectively. We show below (footnote 5) that the total number of Oort-cloud comets with semimajor axes in the range specified by $[L, L + dL]$ is $(2\pi)^3 f(L)L^2 dL$; this in turn implies that the number density of comets is $\propto r^\alpha$ for $a_- \ll r \ll a_+$.

Simulations of the formation of the Oort cloud by Duncan *et al.* (1987) suggest that the number density of Oort-cloud comets is $\propto r^{-(3.5\pm0.5)}$ between 3000 and 50,000 AU. Thus we set $\alpha = -3.5$, $a_- = 10,000$ AU, and $a_+ = 50,000$ AU. The inner edge of the cloud was placed at 10,000 AU instead of 3000 AU because comets with $a < 10,000$ AU cannot become visible except in occasional comet showers, yet would consume most of the computer time in our simulation.

If the comets are uniformly distributed on the energy hypersurface, the fraction of cloud comets with perihelion less than $q \ll a$ is $J^2(q)/L^2 = 2q/a = 0.003(q/40 \text{ AU})(25\,000 \text{ AU}/a)$ (which is consistent with $\int N(q)\,dq$ as given by Eq. (4)). Since the effects of the planets decline rapidly to zero when $q \gtrsim 40$ AU, only a small fraction of cloud comets are influenced by planetary perturbations. Therefore to avoid wasting computer time we

---

[4] Traditionally, the term "nongravitational forces" has been reserved for the reaction forces resulting from the uneven sublimation of cometary volatiles, and it will be used here in that manner. Other factors of a nongravitational nature, including radiation and solar wind pressure, drag from the interplanetary/interstellar medium, and the heliopause, are negligible in comparison to the outgassing forces (Wiegert 1996).

analyze the motion of comets with larger perihelion distances analytically, as we now describe.

4.3.2. Orbit-averaged evolution. For comets in the Oort cloud, the tidal potential (19) is much smaller than the Kepler Hamiltonian $H_{\text{Kep}} = -\frac{1}{2} GM_\odot/a$. Thus the evolution of the comet under the Hamiltonian $H_{\text{Kep}} + V_{\text{tide}}$ can be approximately described by averaging V_{tide} over one period of a Kepler orbit to obtain the orbit-averaged Hamiltonian (Heisler and Tremaine 1986)

$$H_{\text{av}} = -\frac{GM_\odot}{2a} + \pi G\rho_0 a^2 \sin^2 \tilde{\iota}(1 - e^2 + 5e^2 \sin^2 \tilde{\omega}); \quad (24)$$

here $\tilde{\iota}$ and $\tilde{\omega}$ are the inclination and argument of perihelion measured in the Galactic frame. It is useful to introduce canonical momenta

$$L \equiv (GM_\odot a)^{1/2}, \quad J = [GM_\odot a(1 - e^2)]^{1/2}, \quad J_{\tilde{z}} = J \cos \tilde{\iota} \quad (25)$$

and their conjugate coordinates

$$l, \quad \tilde{\omega}, \quad \tilde{\Omega}. \quad (26)$$

Here J is the usual angular momentum per unit mass, $J_{\tilde{z}}$ is its component normal to the Galactic plane, l is the mean anomaly, and $\tilde{\Omega}$ is the longitude of the ascending node on the Galactic plane.[5] In terms of the canonical coordinates and momenta the orbit-averaged Hamiltonian is

$$H_{\text{av}} = -\frac{(GM_\odot)^2}{2L^2} + \frac{\pi \rho_0}{GM_\odot^2} \frac{L^2}{J^2}$$
$$\times (J^2 - J_{\tilde{z}}^2)[J^2 + 5(L^2 - J^2) \sin^2 \tilde{\omega}]. \quad (27)$$

The canonical variables l and $\tilde{\Omega}$ are absent from Eq. (27), so the conjugate momenta L and $J_{\tilde{z}}$ are conserved. The conservation of L implies that semimajor axis is conserved as well. The solution of the equations of motion of (27) is discussed by Heisler and Tremaine (1986) and Matese and Whitman (1989) but is not needed for our purposes.

The rate of change of angular momentum is given by

$$\dot{J} = -\frac{\partial H_{\text{av}}}{\partial \tilde{\omega}}, \quad (28)$$

$$= -\frac{5\pi \rho_0}{GM_\odot^2} \frac{L^2}{J^2} (J^2 - J_{\tilde{z}}^2)(L^2 - J^2) \sin 2\tilde{\omega}, \quad (29)$$

$$= -\frac{5\pi \rho_0}{GM_\odot^2} e^2 L^4 \sin^2 \tilde{\iota} \sin 2\tilde{\omega}, \quad (30)$$

[5] At this point we may prove a result mentioned in Section 4.3.1: if the phase-space density is $f = f(L)$ then the total number of comets in the range $[L, L + dL]$ is $dN = f(L) dL \int_0^L dJ \int_{-J}^J dJ_{\tilde{z}} \int_0^{2\pi} d\tilde{\Omega} \int_0^{2\pi} d\tilde{\omega} \int_0^{2\pi} dl = (2\pi)^3 f(L) L^2 dL$.

Under the influence of the tide, the perihelia of some comets evolve into the near-planetary region. At this point, the "tide-only" approximation that we have used so far breaks down, and a full numerical integration of the cometary path must be begun. This transition must be made *before* the planets begin to significantly influence the comets' orbits. With this in mind, we define the "entrance surface" to be the boundary of the region of phase space with $J \leq J_E(a) \equiv [2GM_\odot q_E(a)]^{1/2}$. We shall integrate individual cometary orbits only after they cross the entrance surface. We choose $q_E = \max(q_1, q_2)$ where q_1 and q_2 reflect two criteria that must be satisfied by the entrance surface: (1) Planetary perturbations must be negligible outside the entrance surface; we take $q_1 = 60$ AU since outside this perihelion distance the RMS fractional energy change per orbit caused by the planets is $\lesssim 0.1\%$ for a typical Oort-cloud comet. (2) The orbit-averaged approximation for the effects of the Galactic tide must be reasonably accurate outside the entrance surface; thus we demand that J_E must exceed $\eta > 1$ times the maximum change in angular momentum per orbit, which in turn requires

$$J_E(L) \geq \eta \frac{10\pi^2 \rho_0}{G^3 M_\odot^4} L^7, \quad \text{or} \quad q_2 = \eta^2 \frac{50\pi^4 \rho_0^2}{M_\odot^2} a^7, \quad (31)$$

where we have assumed $e \sim 1$. In this paper we take $\eta = 3$.

The semimajor axis $a_{1,2}$ where $q_1 = q_2$ is

$$a_{1,2} = \left(\frac{M_\odot^2 q_1}{50\pi^4 \eta^2 \rho_0^2} \right)^{1/7}, \quad (32)$$

$$= 2.41 \times 10^4 \text{AU} \left(\frac{\eta}{3} \right)^{-2/7} \left(\frac{q_1}{60 \text{ AU}} \right)^{1/7}$$

$$\times \left(\frac{\rho_0}{0.15 \text{ M}_\odot \text{ pc}^{-3}} \right)^{-2/7}. \quad (33)$$

Thus

$$q_E = \begin{cases} 60 \text{ AU} & \text{where } a \leq a_{1,2} \\ 60 \text{ AU} \left(\frac{a}{a_{1,2}} \right)^7 & \text{where } a > a_{1,2} \end{cases} \quad (34)$$

4.3.3. The flux of comets into the entrance surface. We have assumed in Section 4.3.1 that the phase-space density is a function only of energy or semimajor axis, $f = f(L)$. This assumption is not in general correct for small angular momentum, where the comets are removed by planetary encounters. However, all we require is the flux into the entrance surface, most of which arises from comets whose angular momentum is steadily decreasing under the influence of the Galactic tide. Such comets are unaffected by the planets until after they cross the entrance surface, and hence the assumption that $f = f(L)$ should be approximately correct.

Let $\Phi(L, J_E, J_{\tilde{z}}, \tilde{\Omega}, \tilde{\omega}, l) dL \, dJ_{\tilde{z}} \, d\tilde{\Omega} \, d\tilde{\omega} \, dl$ be the flux of Oort-cloud comets crossing into the entrance surface J_E at a given

point. Then from Eq. (29)

$$\Phi(L, J_E, J_{\tilde{z}}, \tilde{\Omega}, \tilde{\omega}, l) = \begin{cases} \dot{J} f(L), & \text{where } \dot{J} < 0 \\ 0 & \text{otherwise} \end{cases}$$

$$= \begin{cases} -\frac{5\pi\rho_0}{GM_\odot^2} \frac{L^2}{J_E^2} f(L) \left(J_E^2 - J_{\tilde{z}}^2\right) \left(L^2 - J_E^2\right) \sin 2\tilde{\omega} & \text{where } \sin 2\tilde{\omega} > 0, \\ 0 & \text{otherwise.} \end{cases}$$

(35)

In our simulations, the initial orbital elements of the comets are drawn from the distribution described by Φ, using the energy distribution (Eq. (23)).

4.4. End-States

End-states may represent the loss or destruction of a comet or simply an intermediate stopping point, from which the simulation can subsequently be restarted. The possible end-states are:

Collision. The distance between the comet and the Sun or one of the giant planets is less than that object's physical radius. To ensure that we detect collisions, when a comet is close to a Solar System body we interpolate between time steps using a Keplerian orbit around that body.

Ejection. The comet is either (*i*) leaving the Solar System on an orbit which is unbound, *i.e.*, parabolic or hyperbolic with respect to the Solar System's barycenter, or (*ii*) has ventured beyond the last closed Hill surface around the Sun, and is thus considered stripped from the Solar System by the action of passing stars, molecular clouds, *etc*. In either case, the simulation is not terminated until the comet is at least 10^5 AU from the Sun, to allow for the possibility that subsequent perturbations will result in the comet losing energy and returning to a "bound" state.

Exceeded age of Solar System. The elapsed time has exceeded the age of the Solar System, 5×10^9 yr.

Exceeded orbit limit. The comet has completed more than 5000 orbits without reaching one of the other end-states. The integration is terminated and the orbital elements are saved for later examination. This is a safeguard to prevent extremely long-lived comets from consuming excessive computer time.

Faded. The comet is considered to have faded through loss of volatiles, splitting, or other mechanisms, and is no longer bright enough to be observed, even if its orbit should carry it close to the Sun or Earth. We shall investigate various empirical models for fading. The fading end-state is not activated in any simulations unless explicitly mentioned in the accompanying text.

Perihelion too large. The comet's perihelion q has evolved beyond some limit, usually taken to be 40 AU, and q is moving outward under the influence of the tide. Such a comet is unlikely to become visible in the near future.

Short-period. The comet's orbital period has decreased below 200 yr: it has become a short-period (SP) comet. Continued planetary perturbations may cause SP comets to evolve back into LP comets, but we shall see that the fraction of comets that reach

this end-state is very small (at most a few percent; see Tables 1 and 3), so former SP comets are not a significant contaminant.

Visible. The comet passes within 3 AU of the Sun for the first time, an event we shall call the first apparition. Such comets continue to evolve, but the first apparition provides a useful intermediate stopping point for the simulations.

5. RESULTS

We follow the trajectories of our sample comets from the time they cross the entrance surface until they reach one of the end-states in Section 4.4. We divide the evolution into two stages: the previsibility stage, which lasts until the comet first becomes visible, that is, until its first passage within 3 AU of the Sun (the first apparition; cf. Section 2.2); and the postvisibility stage, which lasts from the first apparition until the comet reaches one of the other end-states.

We call the set of LP comets at their first apparition the V_1 comets. Similarly, those making their mth apparition are called the V_m comets. The union of the sets of orbital elements $V_1, V_2, \ldots$ is called the V_∞ comets.

We intend to compare the distribution of elements of the V_1 comets to the observed distributions of elements of new comets and the V_∞ comets to the visible LP comets. Note that the V_∞ comets represent all apparitions of a set of Oort-cloud comets that first crossed the entrance cylinder in a given time interval, while the observations yield all the comets passing perihelion in a given time interval—one is a fixed interval of origin and the other is a fixed interval of observation. However, in a steady state these two distributions are the same except for normalization.

For some purposes it is useful to estimate this normalization, i.e., to estimate the time interval to which our simulation corresponds. To do this, we first estimate the number of perihelion passages per year of new comets with $q < q_v = 3$ AU, which we call Φ_{new}. Kresák and Pittich (1978) find the rate of long-period comets passing within Jupiter's orbit (5.2 AU) to be 25 yr^{-1}. Everhart (1967b), taking more careful account of selection effects, found $\sim$60 yr^{-1} with $q \leq 4$ AU, of which roughly 35 yr^{-1} would pass within 3 AU. Assuming one in three of these is dynamically new (Festou *et al.* 1993b), we find $\Phi_{\text{new}} \simeq 12$ yr^{-1}. The number of V_1 comets produced in our simulation (see below) is 1368; hence our simulation corresponds to a time interval

$$t_s \approx 115 \text{ yr} \left(\frac{12 \text{ yr}^{-1}}{\Phi_{\text{new}}} \right). \tag{36}$$

The total number of comets crossing the entrance surface in our simulation is 125,495. Using our assumed form for the semi-major axis distribution of comets in the Oort cloud (Eq. (23), with $\alpha = -3.5$) and our formula for the flux through the entrance cylinder (Eq. (35)), we may deduce that the normalization constant in Eq. (23) is $f_0 = 9 \times 10^{12} (\Phi_{\text{new}}/12 \text{ yr}^{-1})$ in units of $L^{-2\alpha-6} = L$, recalling that the units are years, AU, and $M_\odot$ so

that $G = 4\pi^2$. The total population of the Oort cloud is

$$N_{\text{Oort}} = 2 \times 10^{12} (\Phi_{\text{new}}/12 \text{ yr}^{-1}), \qquad (37)$$

from 10,000 AU to 50,000 AU, or twice as many as from 20,000 AU to 50,000 AU. Extrapolating in to 3000 AU yields a population a factor of 2.5 higher. For comparison, Heisler (1990) found that 0.2 new comets per year with perihelion $<$2 AU are expected per 10^{11} Oort-cloud objects outside 3000 AU. This determination corresponds to an Oort-cloud population of roughly 4×10^{12} objects, which compares favorably to our value of 5×10^{12}. Of course, these estimates depend strongly on uncertain assumptions about the extent of the inner Oort cloud.

5.1. Previsibility Evolution

The dynamically new or V_1 comets can be used as a starting point for any investigation of phenomena that only affect the comet after its first apparition (nongravitational forces, fading, etc.). The elements of the V_1 comets are measured in the barycentric frame 200 AU from the Sun.

The simulations reported here followed the evolution of 125,495 Oort-cloud comets that crossed the entrance surface. The orbital elements at the entrance surface were determined as described in Section 4.3. Of the comets crossing the entrance surface, 84% had minimum perihelion distances (determined from contours of the averaged Hamiltonian in Eq. (27)) greater than 40 AU, too far outside the planetary system to suffer significant ($\gtrsim$1%) perturbations in semimajor axis from the planets. These comets were transferred to the *Perihelion too large* end-state. The orbits of the remaining 20,286 comets were followed in the field of the Galactic tide and the Sun and planets. Table 1 shows the distribution of these comets among the various end-states; 1368 or 6.7% became V_1 comets. Only 57 comets triggered the *Exceeded orbit limit* flag (see Section 4.4), set at 5000 revolutions; these are discussed further in Section 5.1.1.

TABLE 1
The Distribution of End-States of the 20,286 Oort-Cloud Comets with Minimum Perihelia <40 AU

	End state					
	Ejection	Exc. limit	Large q	Short pd.	Visible	Total
Number	3,807	57	15,023	32	1368	20,286
Fraction	0.1877	0.0028	0.7406	0.0015	0.0674	1.0000
Minimum t_x	6.80	17.2	7.46	11.7	7.14	6.80
Median t_x	28.7	152	35.2	29.3	26.8	33.3
Maximum t_x	342	480	1182	72.4	147	1182
Minimum m_x	1	5000	1	6	1	1
Median m_x	8	5000	5	387	5	6
Maximum m_x	4799	5000	4872	3432	2937	5000

Note. The minimum, median, and maximum lifetimes m_x and t_x are shown in orbital periods and Myr, respectively. No comets suffered collisions with the planets or the Sun or survived for the lifetime of the Solar System.

TABLE 2
Planetary Encounter Data during the Previsibility Stage for the 20,286 Oort-Cloud Comets with Minimum Perihelion <40 AU

	Planet				
	Jupiter	Saturn	Uranus	Neptune	Total
Number of comets	60	145	71	67	343
Number of encounters	210	317	109	93	729
Encounters/comet	3.5	2.19	1.53	1.39	2.13
Collisions	0	0	0	0	0
Captures	0	0	0	0	0
Min. distance (R_I)	0.023	0.043	0.074	0.049	0.023
Min. distance (R_p)	16.0	38.7	150	167	16.0
$R_I(R_p)$	674	907	2030	3510	—
Outer satellite (R_p)	326	216	23	222	—

Note. Encounters for the 57 comets in the *Exceeded time limit* end-state are included only up to their 5000th orbit. "Captures" are considered to occur when the comet has a planetocentric eccentricity less than unity at planetocentric pericenter. The radius of the planet's sphere of influence R_I (Eq. (17)) and the semimajor axis of its outermost satellite are also given, in units of the planetary radius R_p.

These computations consumed eight weeks of CPU time on a 200 MHz Alpha workstation.

During the pre-visibility stage there were 729 close encounters (Eq. (17)) with the giant planets by 343 individual comets, distributed as shown in Table 2.

A scatter plot of perihelion distance versus original semimajor axis for the V_1 comets is shown in Fig. 10a. There is a sharp lower bound to the distribution of semimajor axes for comets with perihelion distance, which is due to the Jupiter barrier (Section 3.2). This lower bound shifts to smaller semimajor axes at larger perihelion distances, since the angular momentum "hop" over the Jupiter barrier is smaller. As a result the number of V_1 comets as a function of perihelion distance (Fig. 10b) is approximately flat, as predicted by Eq. (4), but slowly increasing with perihelion distance—a result already obtained by Weissman (1985). A least-squares fit to the distribution gives $N(q) = (57 \pm 2.6) + (7.6 \pm 1.5)q \propto 1 + 0.13q$. In comparison, the distribution of perihelion distances for the observed new comets (Fig. 8a) is not flat, but this is probably a result of the strong selection effects acting against comets with large perihelia.

The distribution of original semimajor axes of the V_1 comets is shown in Fig. 11a. The cutoff at $1/a = 2 \times 10^{-5}$ AU^{-1} or $a = 50,000$ AU is an artifact of our choice of a sharp outer boundary for the Oort cloud at this point (Section 4.3.1). All but 2% of the simulated dynamically new comets have original energies in the range $0 < x < 10^{-4}$ AU^{-1}. The mean energy of the V_1 comets is $\langle 1/a \rangle = 3.3 \pm 1 \times 10^{-5}$ AU^{-1}, in good agreement with Heisler's (1990) estimate of 3.55×10^{-5} AU^{-1} outside of showers. Heisler's Monte Carlo simulations included both the Galactic tide and passing stars; the agreement suggests that our omission of stellar perturbers does not strongly bias the distribution of dynamically new comets. Our result is also consistent with the
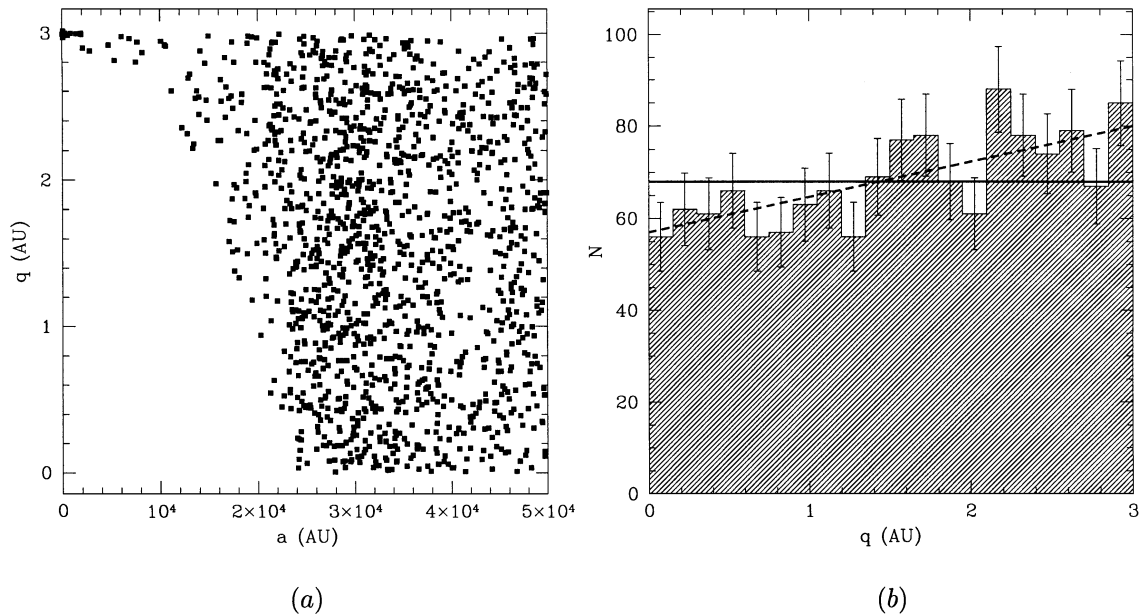
FIG. 10. The V_1 or dynamically new comets: (a) perihelion distance q versus original semimajor axis a; (b) number as a function of perihelion distance. The dashed line indicates the linear least-squares fit to the perihelion distribution, $N(q) \propto 1 + 0.13q$ (see text).

semimajor axis distribution of new comets: taking the 61 new comets with Class I orbits in Marsden *et al.* (1978) and performing a linear least-squares fit to the function $1/a = 1/a_0 + b/q$ (the parameter b accounts for non-gravitational forces, following Marsden *et al.*), we find $1/a_0 = (2.3 \pm 0.7) \times 10^{-5}$ AU^{-1}. Marsden *et al.* find $1/a_0 = (4.6 \pm 0.1) \times 10^{-5}$ AU^{-1} but we are unable to reproduce this result.

The curve in Fig. 11b shows an analytical approximation to the expected flux of new comets when the loss cylinder is full (Wiegert 1996). The agreement between the analytical curve and the distribution of V_1 comets for $a \gtrsim 30{,}000$ AU confirms that the inner edge of the distribution of dynamically new comets is caused by the emptying of the loss cylinder as the semimajor axis decreases. The source of the smaller peak at 47,000 AU
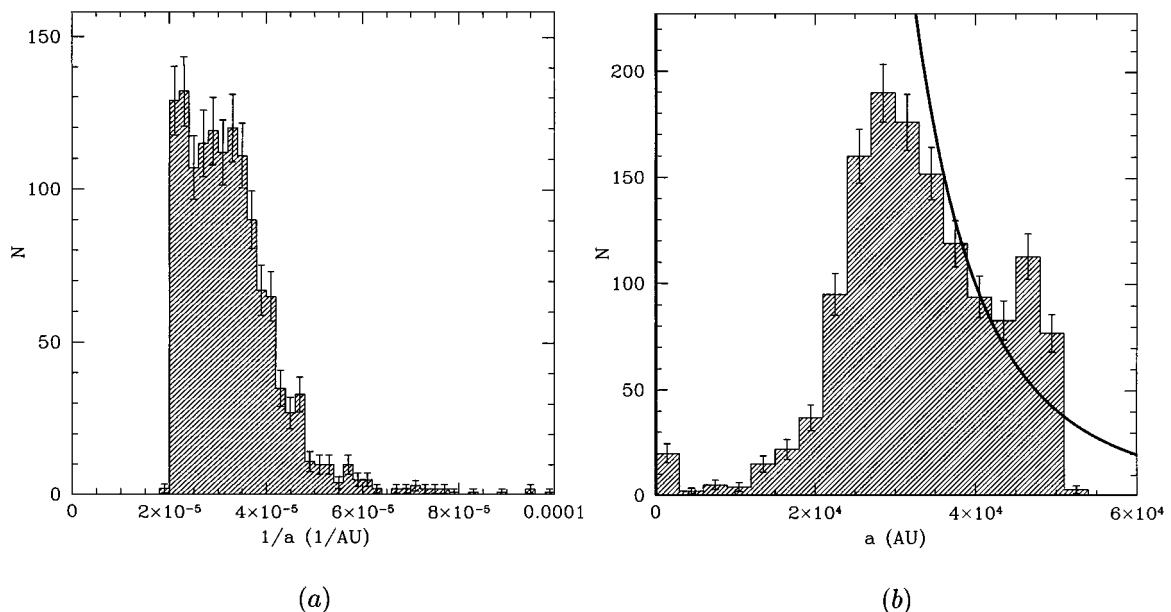

FIG. 11. Distribution of original energies $x = 1/a$ and semimajor axes a for the V_1 comets. An additional 28 comets, 2% of the total, have $x > 10^{-4}$ AU^{-1}. The curve in (b) is an analytical approximation to the expected distribution when the loss cylinder is full, derived in Wiegert (1996).
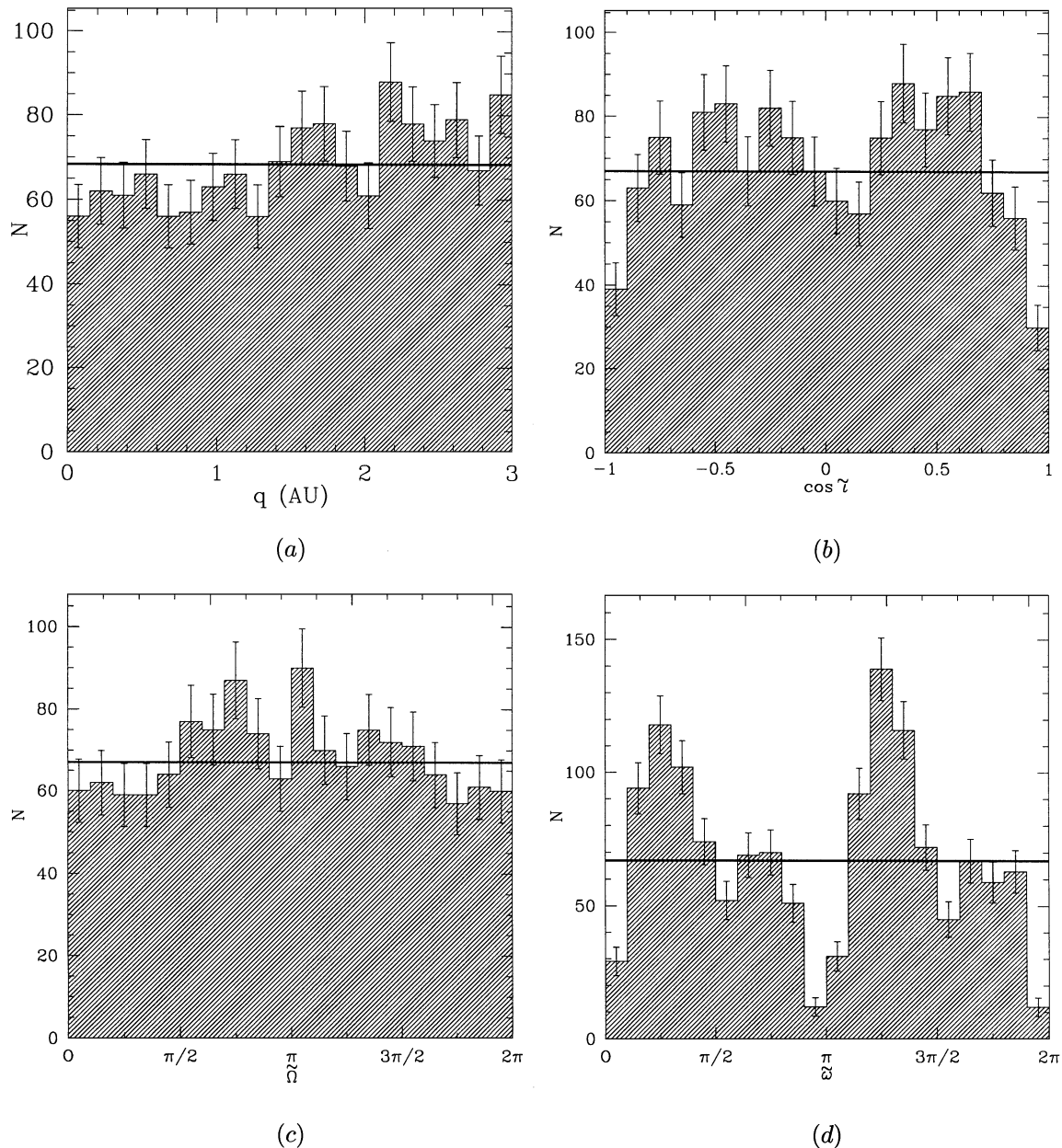
FIG. 12. Distribution of orbital elements for the V_1 comets: (a) perihelion distance; (b) inclination; (c) longitude of ascending node; (d) argument of perihelion. All angular elements are measured in the Galactic frame when the comet passes 200 AU on its inbound leg.

is unclear: if the sample is split into two parts, it appears only in one, and thus may be a statistical fluke even though the deviation from the analytical curve is several times the error bars. In any event it is unlikely to play a significant role in determining the overall distribution of LP comets for two reasons: first, only a few percent of the V_1 comets are involved in the peak; and second the subsequent planet-dominated evolution of the V_1 comets is relatively insensitive to the comets' original semimajor axes.

The distributions of perihelion and angular orbital elements for the V_1 comets are shown in Fig. 12, which can be compared to the observed distributions in Fig. 8. The observed perihelion distribution is strongly affected by selection effects, so no comparison is practical there. The angular element distributions are reasonably consistent between the two figures. In particular the $\tilde{\omega}$ distributions both show peaks in the regions where $\sin 2\tilde{\omega} > 0$, reflecting the role of the Galactic tide in creating new comets.

The aphelion directions of the V_1 comets are shown in Fig. 13, which can be compared to the observed distribution in Fig. 9. The most striking feature in Fig. 13 is the concentration towards mid-Galactic latitudes, again pointing to the importance of the
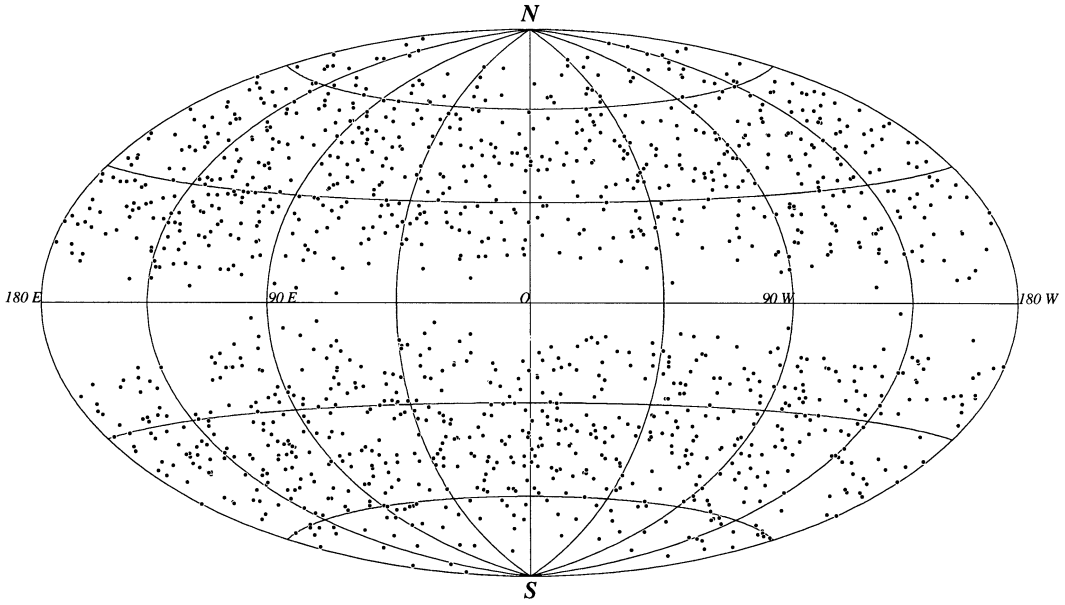
FIG. 13. Equal-area plot of the aphelion directions of the V_1 comets in the Galactic frame. More precisely, we have plotted the antipode of the perihelion direction, since this is what is observable.

Galactic tide as a LP comet injector. The real distribution of aphelion directions is expected to contain an additional fairly uniform component as well, due to the injection of comets by passing stars (Weissman 1996a); however, the number of dynamically new comets in Fig. 9 is too small for any reliable comparisons to be made.

5.1.1. The longest-lived comets. Although most comets reach one of the end-states within a few orbits (see Table 1)

a small fraction survive for much longer times: 57 of the 20,286 initial comets in our simulation triggered the *Exceeded orbit limit* flag after 5000 orbits. The population of these comets decays only very slowly and their fate cannot be determined without prohibitive expenditures of CPU time. The perihelion distances and semimajor axes of these comets on their 5000th orbit are indicated in Fig. 14. Also shown is the distance at which they cross the ecliptic. Most have nodes and perihelia outside Saturn's orbit, where the energy perturbations are relatively small.
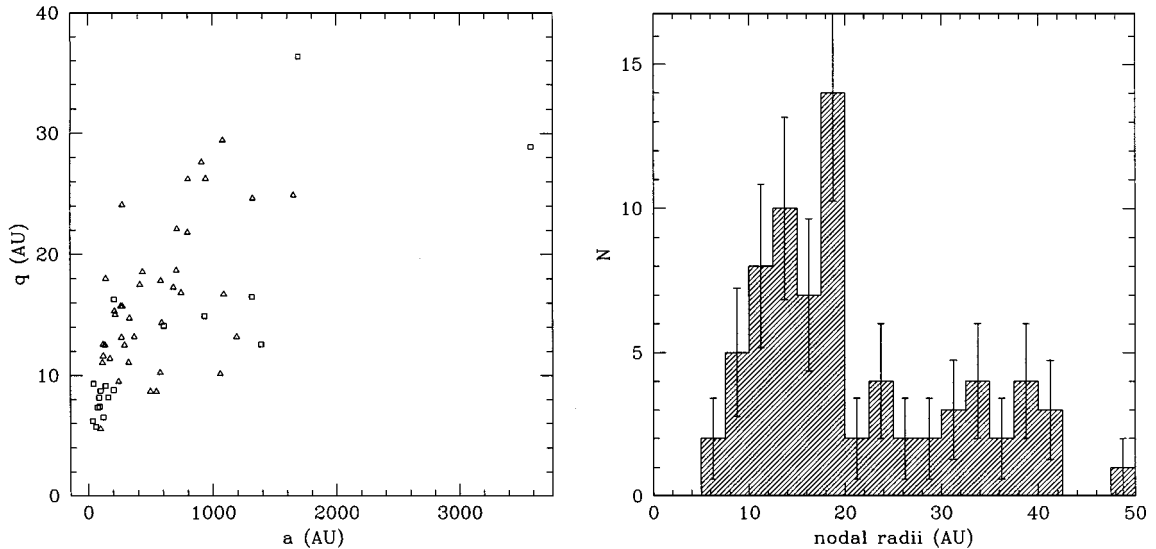

FIG. 14. For the 57 comets that survived 5000 orbits, we plot (a) their perihelion distance q versus semimajor axis a, and (b) the distances of their nodes. In (a), triangles are prograde comets, squares, retrograde.

5.2. Postvisibility Evolution: The Standard Model

We now follow the orbits of the V_1 comets forward in time until they reach one of the end-states (obviously, the *Visible* end-state is disabled in these simulations). Each time one of these comets makes an apparition its orbital elements are added to the set of V_∞ comets. The V_∞ comets are to be compared to the observed distribution of LP comets.

The errors in the distribution of elements of the V_∞ comets are not Poisson, as a single comet may contribute hundreds or thousands of apparitions. The errors that we quote and show in the figures are determined instead by bootstrap estimation (Efron 1982; Press *et al.* 1992).

The "standard model" simulation of post-visibility evolution has no fading, and no perturbers except the giant planets and the Galactic tide.

The distribution of end-states for the standard model is shown in Table 3. The *Exceeded orbit limit* end-state (Section 4.4) is invoked after 10,000 orbits for these simulations, but no comets reach this end-state. The mean lifetime is 45.3 orbits, compared to 60 predicted by the gambler's ruin model (Eq. (8)); this is rather good agreement considering the approximations involved in deriving the latter model. Ejection by the giant planets is by far the most common end-state (89% of V_1 comets). Most of the remaining comets (about 8% of the total) move back out to large perihelion distances. Their median energy when they reach this end-state is given by $1/a = 4 \times 10^{-5}$ AU^{-1} ($a = 25,000$ AU); in other words these comets have suffered relatively small energy perturbations and remain in the outer Oort cloud.

The distribution of orbital elements of the V_∞ comets may be parametrized by the dimensionless ratios X_i defined in Eq. (3): the ratio of theoretical parameters Ψ_i^t for the standard model to the observed parameters (Eq. (3)) is

$$X_1 = \frac{\Psi_1^t}{\Psi_1} = 0.075 \pm 0.011, \quad X_2 = \frac{\Psi_2^t}{\Psi_2} = 4.4 \pm 1.2,$$

$$X_3 = \frac{\Psi_3^t}{\Psi_3} = 0.61 \pm 0.13. \tag{38}$$

TABLE 3
The Distribution of End-States of the V_1 Comets in the Standard Model

	End state			
	Ejection	Large q	Short pd.	Total
Number	1223	109	36	1368
Fraction	0.894	0.080	0.026	1.000
Minimum t_x	0.296	2.61	0.014	0.014
Median t_x	1.33	4.62	0.67	1.40
Maximum t_x	31.7	71.0	7.94	71.0
Minimum m_x	1	1	13	1
Median m_x	1	2	330	1
Maximum m_x	5832	2158	4277	5832

Note. The minimum, median, and maximum lifetimes t_x of these comets are measured in Myr from their first apparition. No comets suffer collisions with the planets or Sun or survive for the age of the Solar System.
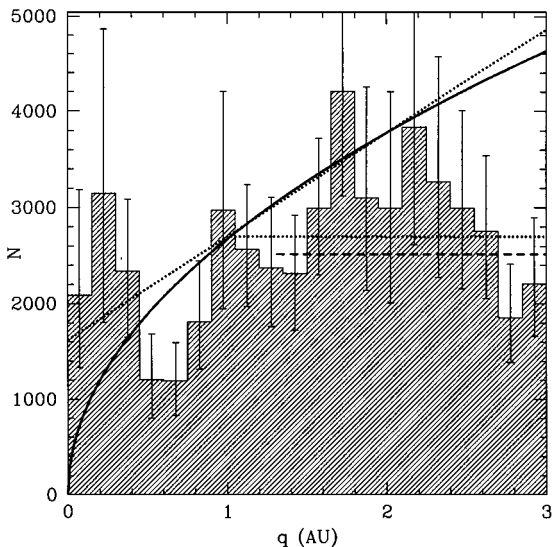

FIG. 15. Distribution of perihelion distances q for the V_∞ comets in the standard model. Error bars are determined from bootstrap estimators and represent one standard deviation. The curves are Everhart's (1967a, dotted line), Kresák and Pittich's (1982, solid line) and Shoemaker and Wolfe's (1982, dashed line) estimates of the intrinsic perihelion distribution. The correct normalizations are unclear, and have been chosen arbitrarily for plotting purposes.

The standard model agrees much better with the predictions of the simple gambler's ruin model ($X_1 = 0.05$, $X_3 = 0.58$, see Eqs. (11) and (12)) than it does with the observations ($X_i = 1$). The gamblers' ruin problem thus provides a reasonable analogue to the standard model.

The perihelion distribution of the V_∞ comets in the standard model is shown in Fig. 15. Although the figure represents 52,303 apparitions, the error bars—as determined by bootstrap—remain large, reflecting strong contributions from a few long-lived comets: over 45% of the apparitions are due to the 12 comets that survive for 1000 or more orbits after their first apparition. This figure can be compared to the observed perihelion distribution (Fig. 2), which however reflects the strong selection effects favoring objects near the Sun or the Earth. We note that not all perihelion passages made by comets after their first apparition are visible: in addition to the 52,303 apparitions made by the V_∞ comets, there were 9561 perihelion passages with $q > 3$ AU.

Let the total number of comets with perihelia in the range $[q, q + dq]$ be $N(q)\,dq$. The perihelion distribution is not flat, as would be expected if the distribution were uniform on the energy hypersurface (Eq. (4)). The simulations are noisy enough to be consistent with any number of slowly varying functions of perihelion over $0 < q < 3$ AU, possibly including $N(q) \propto q^{1/2}$, as proposed by Kresák and Pittich (1978). The estimates of the intrinsic perihelion distribution of LP comets published by Everhart, by Kresák and Pittich, and by Shoemaker and Wolfe are indicated on Fig. 15.

The original energy distribution of the V_∞ comets in the standard model is shown in Fig. 16, at two different magnifications, for all 52,303 apparitions. These figures should be compared
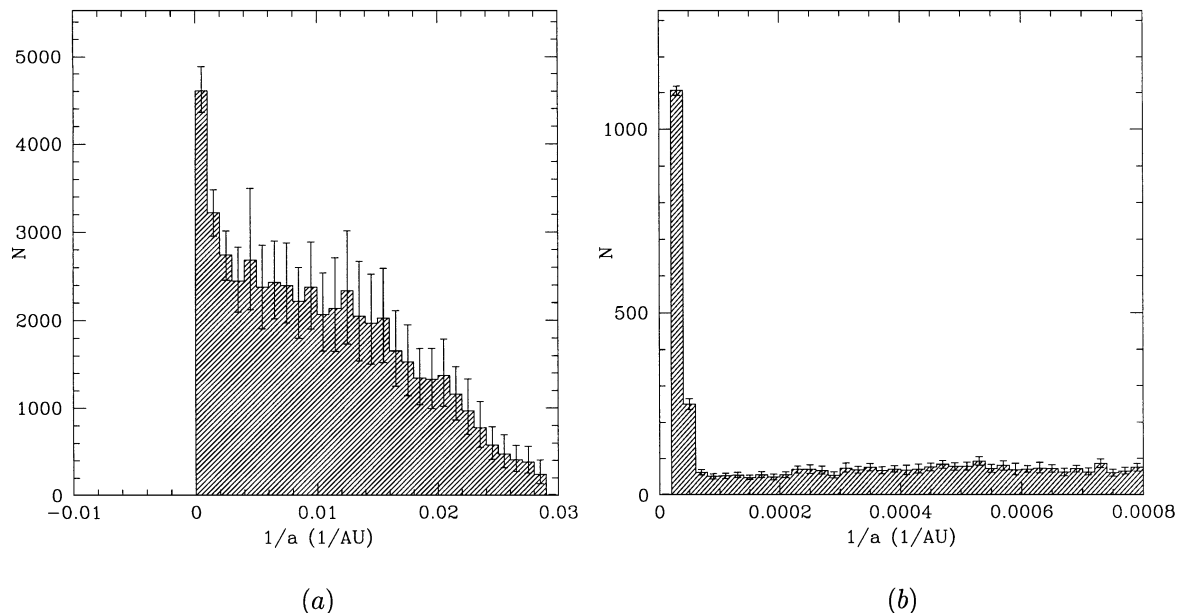
FIG. 16. Distribution of original energies for the V_∞ comets in the standard model for all 52,303 apparitions ($q < 3$ AU).

with the observations shown in Fig. 1. As already indicated by the statistic X_1 (Eq. (38)), the standard model has far too many LP comets relative to the number of comets in the Oort spike: the simulation produces 35 visible LP comets for each comet in the spike, whereas in the observed sample the ratio is 3:1. This disagreement is at the heart of the fading problem: how can the loss of over 90% of the older LP comets be explained?

These simulations allow us to estimate the contamination of the Oort spike by dynamically older comets. There are 1368 V_1 comets, of which 1340 have $1/a < 10^{-4}$ AU^{-1}, but a total of 1475 apparitions are made in this energy range in the standard model. Thus roughly 7% of comets in the Oort spike are not dynamically new, remarkably close to Weissman's (1978) estimate of 8%. Our estimate neglects fading, which would further decrease the contamination of the Oort spike by older comets.

Figure 17 shows the inclination distribution of the V_∞ comets in the standard model. There is a noticeable excess of comets in ecliptic retrograde orbits: the fraction on prograde orbits is $15{,}875/52{,}303 \approx 0.3$. This is inconsistent with observations, which show a roughly isotropic distribution (Fig. 3a), but consistent with the predictions of the gambler's ruin model (Eq. (12)).

Figure 18 shows the distribution of the longitude of the ascending node and the argument of perihelion, in the ecliptic frame. The large error bars suggest that the structure in these figures is probably not statistically significant.

The principal conclusion from this analysis is that the standard, purely dynamical model provides a poor fit to the observed distribution of LP comets. The standard model agrees much better with models based on a one-dimensional random walk, suggesting that the basic assumptions of the analytic random-walk models in Section 3.3 accurately describe the dynamical evolution of the LP comets—even though they neglect the evolution of all orbital elements except semi-major axis, ignore close en-

counters, and replace deterministic evolution with a stochastic process. In Sections 5.3–5.5 we shall explore whether variants of the standard model can provide a better match to the observations.

5.2.1. Short-period comets from the Oort cloud. During our simulations only 68 Oort-cloud comets eventually became SP comets, 36 of them after having made one or more apparitions as LP comets. The distributions of inverse semimajor axis, perihelion distance, and inclination for these comets are shown in Fig. 19. In no case is an Oort-cloud comet converted to an SP comet in a single perihelion passage: the largest orbit at the previous aphelion has a semimajor axis of only 1850 AU. There is a distinct concentration of orbits near zero ecliptic inclination, as expected from studies of captures by Jupiter (Everhart 1972), but the concentration is much less than that of SP comets in our Solar System. The prograde fraction is $44/68 \simeq 0.65$.

Our simulation corresponds to approximately 115 years of real time (Eq. (36)). Thus we deduce that $68/115 \simeq 0.6$ SP comets per year arrive (indirectly) from the Oort cloud (in the absence of fading). For comparison, on average five new SP comets are discovered each year (Festou *et al.* 1993a); we conclude that the Oort cloud contributes of order 10% of the population of SP comets, and another source, such as the Kuiper belt, is required. Only about 10% of the known SP comet apparitions are Halley-family, and thus the Oort cloud may contribute a significant fraction of these objects, though the picture is clouded by the multiple apparitions by individual comets in this sample.

5.2.2. Planetary encounter rates. Close encounters of the V_∞ comets with the giant planets are described in Table 4. Note that multiple encounters between a giant planet and a single
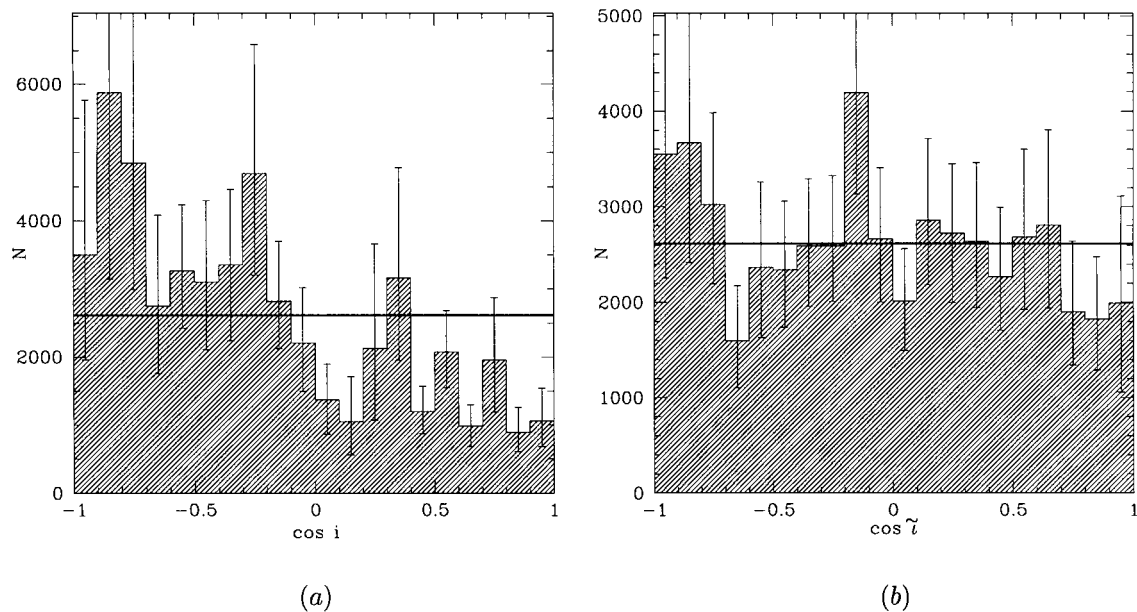
FIG. 17. Distribution of the cosine of the inclination for the V_∞ comets in the standard model (a) at perihelion in the ecliptic frame and (b) at 200 AU on the inbound leg in the Galactic frame. The heavy line indicates a uniform distribution.

comet do not necessarily indicate capture by the planet in the traditional sense (*i.e.*, planetocentric eccentricity less than unity).

Since our simulation corresponds to roughly 115 years of real time (Eq. (36)) we can calculate the rate of close encounters between the LP comets and the giant planets. During the combined pre- and postvisibility phases of the comets' evolution, a total of 253 encounters were recorded for Jupiter, 333 for Saturn, 111

for Uranus, and 96 for Neptune. These numbers translate to total fluxes $\mathcal{J}_p$ of 2.2, 2.9, 0.97, and 0.83 comets per year passing through the spheres of influence (Eq. (17)) of Jupiter through Neptune respectively.

If we assume that these $\mathcal{J}_p$ reflect a uniform flux of LP comets across the sphere of influence of each planet, then the rate of impacts between LP comets and the giant planets can be deduced

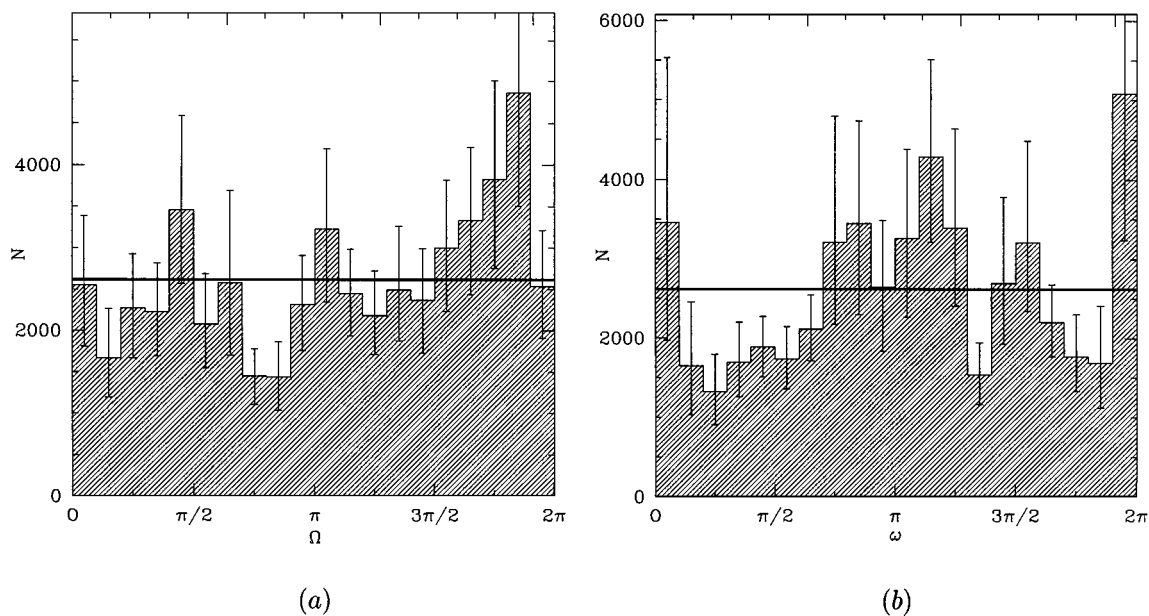**FIG. 18.** Distribution of the longitude of the ascending node and the argument of perihelion for the V_∞ comets in the standard model. The elements are measured at perihelion in the ecliptic frame. The heavy line indicates a uniform distribution.
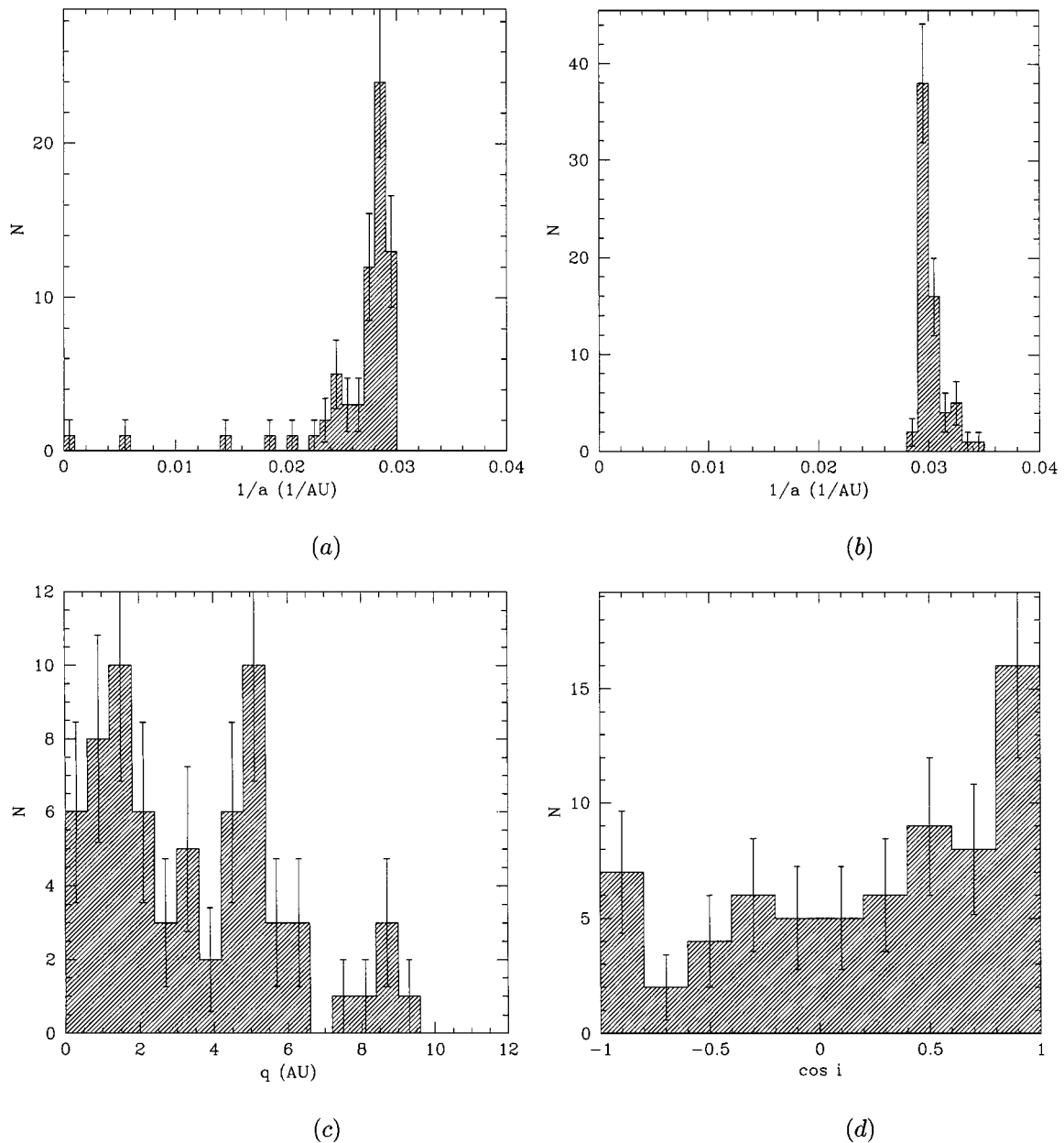
FIG. 19. The distribution of the inverse semimajor axis $1/a$, perihelion distance q, and cosine of the ecliptic inclination i for the SP comets originating in the Oort cloud. The distribution of $1/a$ on the left (a, c) is measured at the aphelion previous to, and the others (b, d) at, the initial perihelion passage as an SP comet.

to be

$$n_p = \mathcal{J}_p \left(\frac{M_p}{M_\odot} \right)^{-4/5} \left(\frac{R_p}{a_p} \right)^2 \left(1 + \frac{2}{3} \frac{M_p}{M_\odot} \frac{a_p}{R_p} \right), \quad (39)$$

where a_p and R_p are the planet's semimajor axis and radius, M_p is the planetary mass, and the second term is a crude correction for gravitational focusing, assuming the comets are on nearly parabolic orbits. The resulting collision rates are 4.0×10^{-5}, 2.0×10^{-5}, 1×10^{-6}, and 5×10^{-7} per year for Jupiter through Neptune respectively. It should be noted that Comet Shoemaker-

Levy 9, which collided with Jupiter in July of 1994, was not a LP comet but rather a Jupiter-family comet (Benner and McKinnon 1995).

5.3. Postvisibility Evolution: The Effect of Nongravitational Forces

Asymmetric sublimation of volatiles leads to significant non-gravitational (NG) forces on comets. As described in Section 4.2, we specify NG forces using two parameters A_1 and A_2. The parameter A_1 is proportional to the strength of the radial NG force and is always positive, as outgassing accelerates the comet away

TABLE 4
Planetary and Solar Encounter Data for the V_∞ Comets in the Standard Model (Postvisibility Stage)

			Planet			
	Sun	Jupiter	Saturn	Uranus	Neptune	Total
Number of comets	7	28	12	2	3	52
Number of encounters	16	43	16	4	3	82
Encounters/comet	2.3	1.5	1.3	2.0	1.0	1.6
Collisions	0	0	0	0	0	0
Captures	—	0	0	0	0	0
Min. distance (R_I)	—	0.018	0.086	0.17	0.16	0.018
Min. distance (R_p)	1.61	12.5	77.9	335	553	12.5
Outer satellite (R_p)	—	326	216	23	222	—

Note. The distance to each planet's outermost satellite is given in the last row.

from the Sun. The parameter A_2 is proportional to the strength of the tangential force, is generally less than A_1, and may have either sign depending on the comet's rotation. Comet nuclei are likely to have randomly oriented axes of rotation, with a corresponding random value of A_2. Rather than make a complete exploration of the available parameter space for A_1 and A_2, we shall investigate a few representative cases.

We assume that $|A_2| = 0.1A_1$, and consider two distributions for the sign of A_2:

1. Half the comets have positive values of A_2, half negative, and the sign of A_2 is constant throughout a comet's lifetime—as if the axis of rotation of the nucleus remained steady throughout the comet's dynamical lifetime. This choice seems unlikely, and indeed Weissman (1978; 1979) showed that it produced too many small perihelion SP comets, but it is examined here for the sake of completeness.

2. The sign of A_2 is chosen at random after each perihelion passage—as if the axis of rotation changed rapidly and chaotically.

We examined four values of A_1: 10^{-8}, 10^{-7}, 10^{-6}, and 10^{-5} AU day^{-2}. The first two of these are reasonably consistent with the NG forces observed in LP comets (Marsden *et al.* 1973). The two remaining values for A_1 are probably unrealistically large, but allow us to explore the effects of unknown forces with the same qualitative behavior as NG forces.

Figure 20 and Table 5 illustrate the effects of NG forces on the energy and perihelion distributions, and on the parameters X_i defined in Eq. (3), which should be unity if the simulated and observed element distributions agree. The figure shows that NG forces do decrease the number of dynamically older comets relative to the number of new comets and hence improve agreement with the observations (*i.e.,* increasing X_1, decreasing X_2); however, the same forces erode the population of comets at small perihelion distances, thereby worsening the agreement with the observed perihelion distribution. Even unrealistically large NG forces cannot bring the distribution of inverse semimajor axes

into line with observations, and these produce an extremely unrealistic depletion of comets at small perihelia.

The effects of NG forces, as modeled here, can be summarized as follows:

- The semimajor axis perturbation due to radial NG forces averages to zero over a full orbit (assuming that the radial force is symmetric about perihelion, as in the model discussed in Section 4.2). Thus radial forces have little or no long-term effect on the orbital distribution.
- Positive values of the tangential acceleration A_2 reduce the tail of the population, resulting in an increase in X_1 toward unity and improving the match with observations, but erode the population at small perihelia, a depletion which is not seen in the observed sample.
- Negative values of A_2 preserve a reasonable perihelion distribution, but increase the number of comets in the tail of the energy distribution, thus reducing X_1 so that the disagreement between the observed and simulated energy distribution becomes even worse.

We have also conducted simulations with a more realistic model for observational selection effects (Eq. (1)) but this does not alter our conclusions.

Although we have not exhaustively explored the effects of NG forces on the LP comet distribution (in particular, we have not explored alternatives to the NG forces in Eqs. (21) and (22) (*e.g.*, Yeomans 1986b)), we are confident that conventional models of NG forces cannot by themselves resolve the discrepancy between the observed and predicted LP comet distribution.

TABLE 5
Parameters of the Distribution of V_∞ Comets Subjected to Nongravitational Forces

A_1	A_2	Total	Spike	Tail	Prograde	X_1	X_2	X_3	$\langle m \rangle$
0.0	0.0	52,303	1,473	15,004	15,875	0.07	4.37	0.61	45.4
1.0	0.1	35,370	1,457	7,368	12,381	0.11	3.17	0.69	36.1
1.0	−0.1	57,819	1,462	19,364	21,110	0.07	5.10	0.72	51.0
1.0	±0.1[a]	44,383	1,461	13,705	19,021	0.09	4.70	0.86	38.4
10	±1[a]	45,899	1,425	16,628	18,504	0.08	4.42	0.80	42.5
100	±10[a]	30,660	1,341	11,296	11,012	0.12	5.61	0.71	33.1
1000	±100[a]	13,248	995	5,432	5,872	0.20	6.24	0.87	14.4
1.0	±0.1[b]	49,642	1,450	13,203	16,387	0.08	4.05	0.65	46.7
10	±1[b]	45,202	1,448	13,631	17,311	0.08	4.59	0.76	41.4
100	±10[b]	25,774	1,364	4,969	11,452	0.14	2.93	0.88	27.7
1000	±100[b]	9,878	1,035	1,536	5,042	0.28	2.37	1.01	13.2

Note. The superscript [a] indicates that half the sample have positive A_2, half negative; [b] indicates that A_2 has a randomly chosen sign for each perihelion passage. "Total" is the total number of apparitions (*i.e.*, perihelion passages with $q < 3$ AU), "Spike" is the number of these with original inverse semimajor axes $1/a < 10^{-4}$ AU^{-1}, "Tail" is the number with 0.0145 AU$^{-1} < 1/a < 0.029$ AU^{-1}, and "Prograde" is the number with ecliptic inclination less than $90°$. The parameters X_i are defined in Eq. (3). The mean lifetime in orbits $\langle m \rangle$ includes all perihelion passages, whether visible or not, after the initial apparition. The units of A_1 and A_2 are AU day^{-2}.
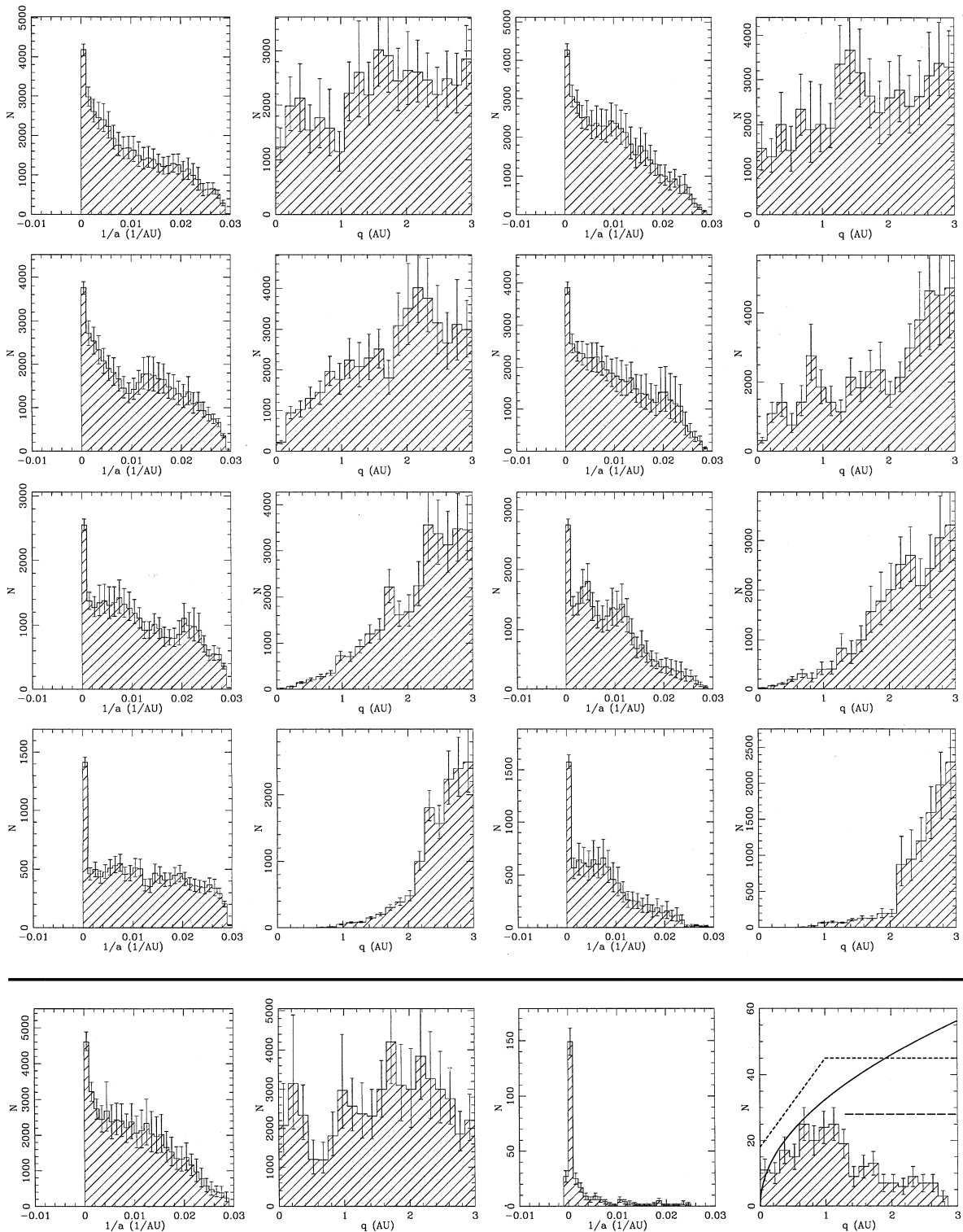
FIG. 20. Distribution of the inverse semimajor axis $1/a$ and perihelion distance q for V_∞ comets subjected to nongravitational forces. Left panels: constant values for A_2, half positive, half negative. Right panels: the sign of A_2 is randomized for each perihelion passage. From the top down, $A_1 = 10^{-8}$, 10^{-7}, 10^{-6}, and 10^{-5} AU day^{-2}, with $|A_2| = 0.1 A_1$. The bottom line of panels is for comparison, and includes the standard model (left side) and the observations (right side). The observed perihelion distribution includes curves indicating the estimated intrinsic distribution (see Fig. 15 for details).

5.4. Postvisibility Evolution: The Effect of a Solar Companion or Disk

In this section we investigate the influence of two hypothetical components of the Solar System on the evolution of LP comets:

1. A massive circumsolar disk extending to hundreds of AU or even further. Such a disk might be an extension of the Kuiper belt (*e.g.*, Weissman 1984; Harper *et al.* 1984) or related to the gas and dust disks that have been detected around stars (especially β Pictoris) and young stellar objects (Ferlet and Vidal-Madjar 1994). Residuals in fits to the orbit of Halley's comet imply that the maximum allowed mass for a disk of radius r around our own Solar System is roughly (Hamid *et al.* 1968; Yeomans 1986a; Hogg *et al.* 1991)

$$M_{\max} \simeq 10 M_{\oplus} \left(\frac{r}{100 \text{ AU}} \right)^3. \qquad (40)$$

Current estimates of the mass in the Kuiper belt are much smaller, typically $\sim 0.1 M_{\oplus}$ from direct detection of 100 km objects (Jewitt *et al.* 1996) or from models of diffuse infrared emission (Good *et al.* 1986; Backman *et al.* 1995), but these are based on the uncertain assumption that most of the belt mass is in the range 30–50 AU. The disk around β Pic is detected in the infrared to radii exceeding 1000 AU (Smith and Terrile 1987); the dust mass is probably less than $1 M_{\oplus}$ (Artymowicz 1994), but there may be more mass in condensed, macroscopic objects.

2. A solar companion, perhaps a massive planet or brown dwarf, orbiting at hundreds of AU. Residuals in fits to the orbits of the outer planets imply that the maximum allowed mass for a companion at radius r is roughly (Tremaine 1990; Hogg *et al.* 1991)

$$M_{\max} \simeq 100 M_{\oplus} \left(\frac{r}{100 \text{ AU}} \right)^3. \qquad (41)$$

There are also significant but model-dependent constraints on the characteristics of a solar companion from the IRAS infrared all-sky survey (Hogg *et al.* 1991).

To reduce computational costs, we used the V_1 comets as a starting point for these investigations; that is, the effect of the disk or companion is ignored before the comet's first apparition (more precisely, we started the integration at the aphelion preceding the comet's initial apparition, in order to correctly calculate any perturbations occurring on the inbound leg). Starting at this point is an undesirable oversimplification, but one that should not compromise our conclusions.

5.4.1. Circumsolar disk. The circumsolar disk is represented by a Miyamoto–Nagai potential (*e.g.*, Binney and Tremaine 1987),

$$V_{\text{disk}}(x, y, z) = \frac{-G M_{\text{d}}}{\left[x^2 + y^2 + \left(a_{\text{d}} + \sqrt{z^2 + b_{\text{d}}^2} \right)^2 \right]^{1/2}}. \qquad (42)$$

Here M_{d} is the disk mass, and a_{d} and b_{d} are parameters describing

the disk's characteristic radius and thickness. We assume that the disk is centered on the Solar System barycenter and coplanar with the ecliptic. We considered disk masses M_{d} of 0.1, 1, and 10 Jupiter masses, disk radii a_{d} of 100 and 1000 AU, and a fixed axis ratio $b_{\text{d}}/a_{\text{d}} = 0.1$. The two more massive disks with $a_{\text{d}} = 100$ AU are unrealistic because they strongly violate the constraint (40), but we examine their effects in order to explore as wide a range of parameters as possible.

Comets arriving from the Oort cloud have fallen through the disk potential and hence are subjected to a shift in their original inverse semimajor axis. This offset can be as large as 2×10^{-4} AU^{-1} for a 10-Jupiter-mass disk with radius 100 AU, but is much smaller for disks that do not already violate the observational constraint (40). This shift is not shown in the figures below, for which the semimajor axis is measured at aphelion.

As usual, the *Perihelion too large* end-state (Section 4.4) was entered if $q > 40$ AU and $\sin 2\tilde{\omega} > 0$. The assumption that such comets are unlikely to become visible in the future is only correct if the torque is dominated by the Galactic tide, and this may not be the case when a disk is present. However, there is no significant difference in the numbers or semimajor axes of the comets reaching this end-state in simulations with and without a circumsolar disk, suggesting that evolution to this end-state is indeed dominated by the Galaxy.

The results from simulations including a circumsolar disk are displayed in Fig. 21 and Table 6. One plot of the energy distribution in Fig. 21 shows a strong peak near $1/a = 0.02$ AU^{-1}; as the large error bars suggest, this peak is caused by a single comet and has little statistical significance.

The principal effect of the disk is to exert an additional torque on the comets, resulting in oscillations of the comet's perihelion

TABLE 6
Parameters of the Distribution of V_{∞} Comets when the Solar System Contains a Circumsolar Disk

M_{d}	a_{d}	Total	Spike	Tail	Prograde	X_1	X_2	X_3	$\langle m \rangle$	$R_{\odot}$
0	—	52,303	1,473	15,004	15,875	0.07	4.37	0.61	45.4	0
0.1	100	38,947	1,486	8,382	15,178	0.10	3.28	0.77	60.4	0
0.1	1000	42,106	1,496	9,122	16,957	0.09	3.30	0.80	33.7	1
1	100	37,676	1,459	12,027	11,888	0.10	4.86	0.63	60.8	2
1	1000	39,138	1,458	9,944	16,141	0.10	3.87	0.82	44.7	1
10	100	26,445	1,416	8,881	6,813	0.14	5.11	0.51	62.6	5
10	1000	16,636	1,324	3,020	7,555	0.21	2.76	0.90	66.9	3
0^d	—	33,449	957	10,190	14,308	0.09	4.17	0.83	45.5	0
0.1^d	100	24,535	968	6,086	8,589	0.10	3.76	0.69	60.4	0
0.1^d	1000	26,335	969	5,261	11,950	0.10	3.04	0.91	33.7	1
1^d	100	27,655	947	9,514	8,712	0.09	5.24	0.62	60.8	2
1^d	1000	25,200	947	7,070	9,881	0.10	4.27	0.77	44.7	1
10^d	100	18,769	939	7,104	4,103	0.13	5.76	0.44	62.6	5
10^d	1000	10,600	910	1,541	4,650	0.23	2.21	0.85	66.9	3

Note. The disk mass M_{d} is measured in Jupiter masses and the disk radius a_{d} is measured in AU. The rightmost column indicates the number of comets that collided with the Sun. The superscript ^{d} indicates that the discovery probability from Eq. (1) has been applied. The definitions of the other columns are the same as in Table 5.
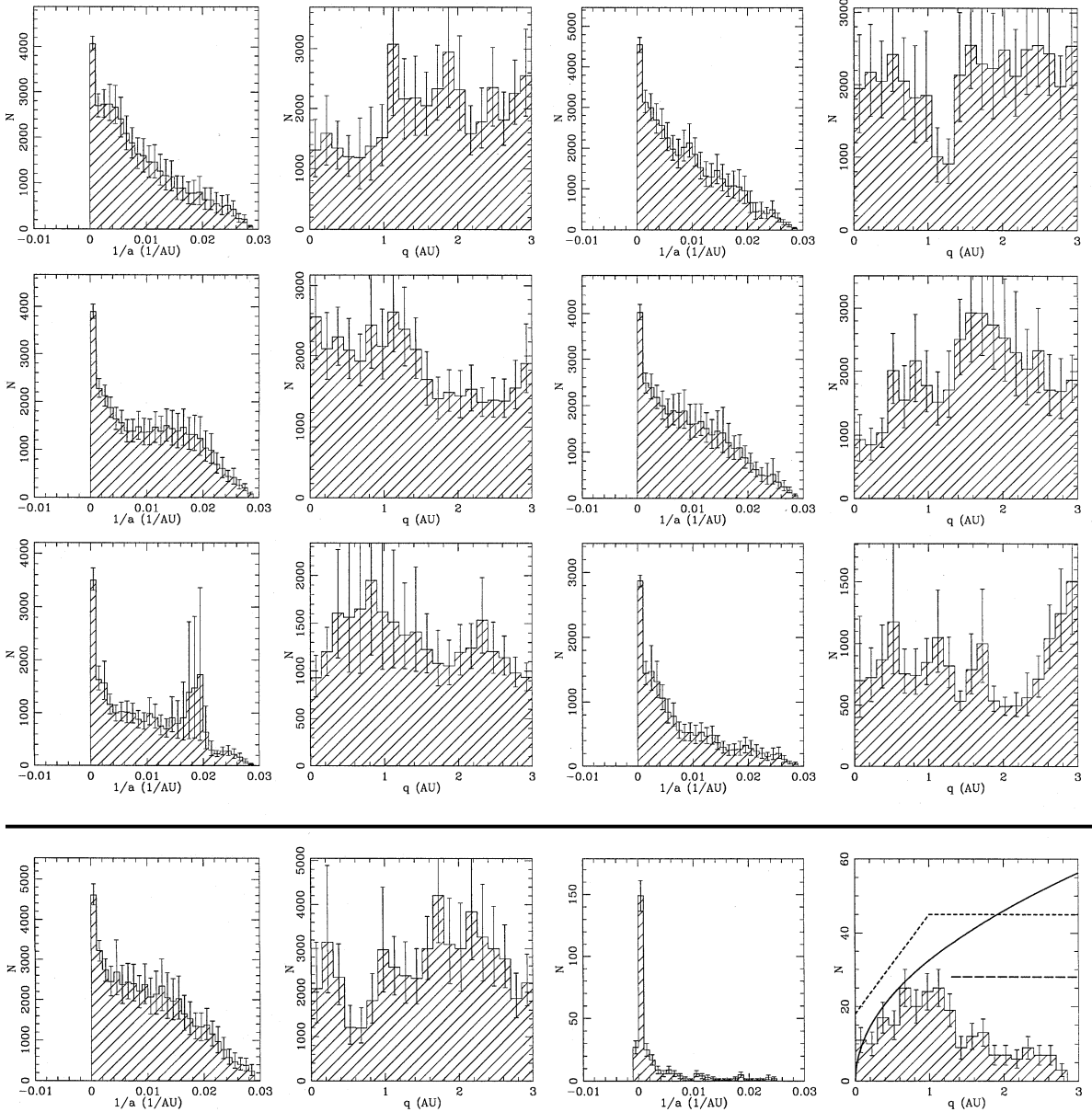
FIG. 21. Distribution of the inverse semimajor axis $1/a$ and perihelion distance q for the V_∞ comets, when the Solar System contains a massive circumsolar disk. Left panels: characteristic disk radius $a_d = 100$ AU. Right panels: disk radius $a_d = 1000$ AU. From the top down, the disk masses are 0.1, 1, and 10 Jupiter masses. The bottom line of panels is for comparison, and includes the standard model (left side) and the observations (right side). The observed perihelion distribution includes curves indicating the estimated intrinsic distribution (see Fig. 15 for details).

distance. This effect normally increased the comet's lifetime, as the risk of ejection is greatly reduced when the comet is outside Saturn's orbit. The perihelion oscillations also enhance the probability of collision with the Sun (Table 6).

The perihelion distribution of visible comets is not strongly affected by the disk. The presence of a massive disk reduces the number of dynamically old comets (because their perihelia are no longer nearly constant, only a fraction of them are visible at any given time), but not enough so that the energy distribution is consistent with the observations. This conclusion is confirmed

by examining the X parameters in Table 6, which should be unity if the simulated element distribution agrees with the observations (cf. Eq. (3)). The values of X_1, which measures the ratio of number of comets in the spike to the total number, are far smaller than unity even for the most massive disks. Increasing the disk mass tends to improve X_2 and X_3 for the 1000 AU disk, but degrades the fit for the 100 AU disk. There is no set of disk parameters than comes close to producing a match with observations. Using a more elaborate model for selection effects (Eq. (1)) does not alter this conclusion (see bottom half of Table 6).

TABLE 7
Parameters of the Distribution of V_∞ Comets when the Solar System Contains a Massive Solar Companion

M_X	a_X	Total	Spike	Tail	Prograde	X_1	X_2	X_3	$\langle m \rangle$	$R_\odot$
0.1	100	40,662	1,451	9,111	14,074	0.11	3.07	0.67	43.1	1
0.1	1000	49,420	1,490	10,057	13,550	0.09	2.79	0.53	44.4	1
1	100	38,397	1,473	7,465	9,379	0.12	2.66	0.47	85.4	4
1	1000	35,940	1,438	9,338	13,544	0.12	3.56	0.73	68.1	1
10	100	14,877	1,379	3,365	5,846	0.28	3.10	0.75	66.0	4
10	1000	28,600	1,400	8,183	15,489	0.15	3.92	1.04	146.3	2
0.1^d	100	25,300	944	6,762	8,893	0.11	3.66	0.68	43.1	1
0.1^d	1000	31,376	975	6,206	8,623	0.09	2.71	0.53	44.4	1
1^d	100	27,918	963	4,764	6,047	0.10	2.34	0.42	85.4	4
1^d	1000	24,740	943	6,713	8,281	0.12	3.72	0.65	68.1	1
10^d	100	9,749	928	2,197	4,059	0.29	3.09	0.80	66.0	4
10^d	1000	22,177	1,030	6,052	12,649	0.14	3.74	1.10	146.3	2

Note. The companion mass M_X is in Jupiter masses, and its orbital radius a_X is measured in AU. The rightmost column indicates the number of comets that collided with the Sun. The superscript ^{d} indicates that the discovery probability from Eq. (1) has been applied. The definitions of the other columns are the same as in Table 5.

We conclude that a circumsolar disk cannot by itself resolve the discrepancy between the observed and predicted LP comet distribution.

5.4.2. Solar companion. For simplicity, we shall assume that the solar companion has a circular orbit in the ecliptic (the orientation and eccentricity of the companion orbit should not strongly affect its influence on the LP comets since the comets are on isotropic, highly eccentric orbits).

We examined companion masses M_X of 0.1, 1, and 10 Jupiter masses and orbital radii of 100 and 1000 AU. The most massive companion at 100 AU is unrealistic because it strongly violates the constraint (41). As in the previous subsection, the original semimajor axes of the comets are measured at aphelion, and thus do not include the energy offset caused by their fall through the companion's gravitational potential.

The results are presented in Fig. 22 and Table 7. The X parameters are listed in Table 7. As the companion mass is increased, the fraction of prograde to total comets (X_3) improves. However, X_1 and X_2 remain far from unity. There is no evidence that a solar companion can significantly improve the agreement between the observed and predicted LP comet distribution.

5.5. Postvisibility Evolution: Fading

The concept of fading was introduced in Sections 3.3 and 3.4. We use the term "fading" to denote any change in the intrinsic physical properties of the comet that would cause it to disappear from the observed sample. Our focus is on modeling the fading process empirically, rather than attempting to elucidate the physical processes involved. The distributions of inverse semimajor axis and ecliptic inclination will serve as our primary fading benchmarks, through the values of the parameters X_1, X_2, and X_3 (Eq. (3)).

We shall generally assume that fading depends only on the number of apparitions (perihelion passages with $q < 3$ AU). We parametrize the fading process by a function Φ_m (cf. Eq. (5)), the probability that a visible new comet survives fading for at least m apparitions (thus $\Phi_1 = 1$).

We shall conduct simulations with and without plausible non-gravitational (NG) forces (§§ 4.2, 5.3). When NG forces are included, we shall use the parameters $A_1 = 10^{-7}$ AU day^{-2}, $A_2 = \pm 10^{-8}$ AU day^{-2}, $A_3 = 0$, with a random sign for A_2 at each perihelion passage (henceforth the "standard NG model").

The most direct way to determine the fading function Φ_m would be to break down the simulated data set into individual distributions, one for each perihelion passage, i.e., $\{V_1, V_2, V_3, \ldots\}$, and then fit the observed distribution of orbital elements to the parameters $\Phi_1, \Phi_2, \ldots$ where $\Phi_{m+1} \leq \Phi_m$. Unfortunately, this problem is poorly conditioned. Instead, we shall experiment with a few simple parametrized fading functions.

5.5.1. One-parameter fading functions. The fading functions we shall examine include:

(a) *Constant lifetime.* Each comet is assigned a fixed lifetime, measured in apparitions. Thus

$$\Phi_m = 1, \quad m \leq m_v, \qquad \Phi_m = 0, \quad m > m_v. \quad (43)$$

(b) *Constant fading probability.* Comets are assigned a fixed probability λ of fading, per apparition. Thus

$$\Phi_m = (1 - \lambda)^{m-1}. \quad (44)$$

(c) *Power law.* The fraction of comets remaining is

$$\Phi_m = m^{-\kappa}, \quad (45)$$

where κ is a positive constant.

We have also investigated fading functions in which Φ depends on the elapsed time t since the first apparition. Such laws are less physically plausible than fading functions based on the number of apparitions, since by far the harshest environment for comets occurs as they pass perihelion; and in fact the functions $\Phi(t)$ that we investigated all produced relatively poor matches to the observations. Fading functions can also be based on the number of perihelion passages—rather than the number of apparitions, i.e., the number of perihelion passages within 3 AU—but these produce results very similar to laws based on the number of apparitions.

The results from the fading laws (43)–(45) are shown in Figs. 23 to 25. The first of these figures displays the X parameters assuming LP comets have a constant lifetime in apparitions (model [a]). The presence or absence of NG forces (bottom vs top panels), or the use of two different visibility criteria (left vs right panels) has very little effect on the results. The spike/total ratio matches observations (i.e., $X_1 = 1$) at $m_v \simeq 10$, but the tail/total ratio is far too low at that point ($X_2 \ll 1$). The tail/total ratio is right at $m_v \simeq 100$, but X_1 is now too low. The ratio X_3 is
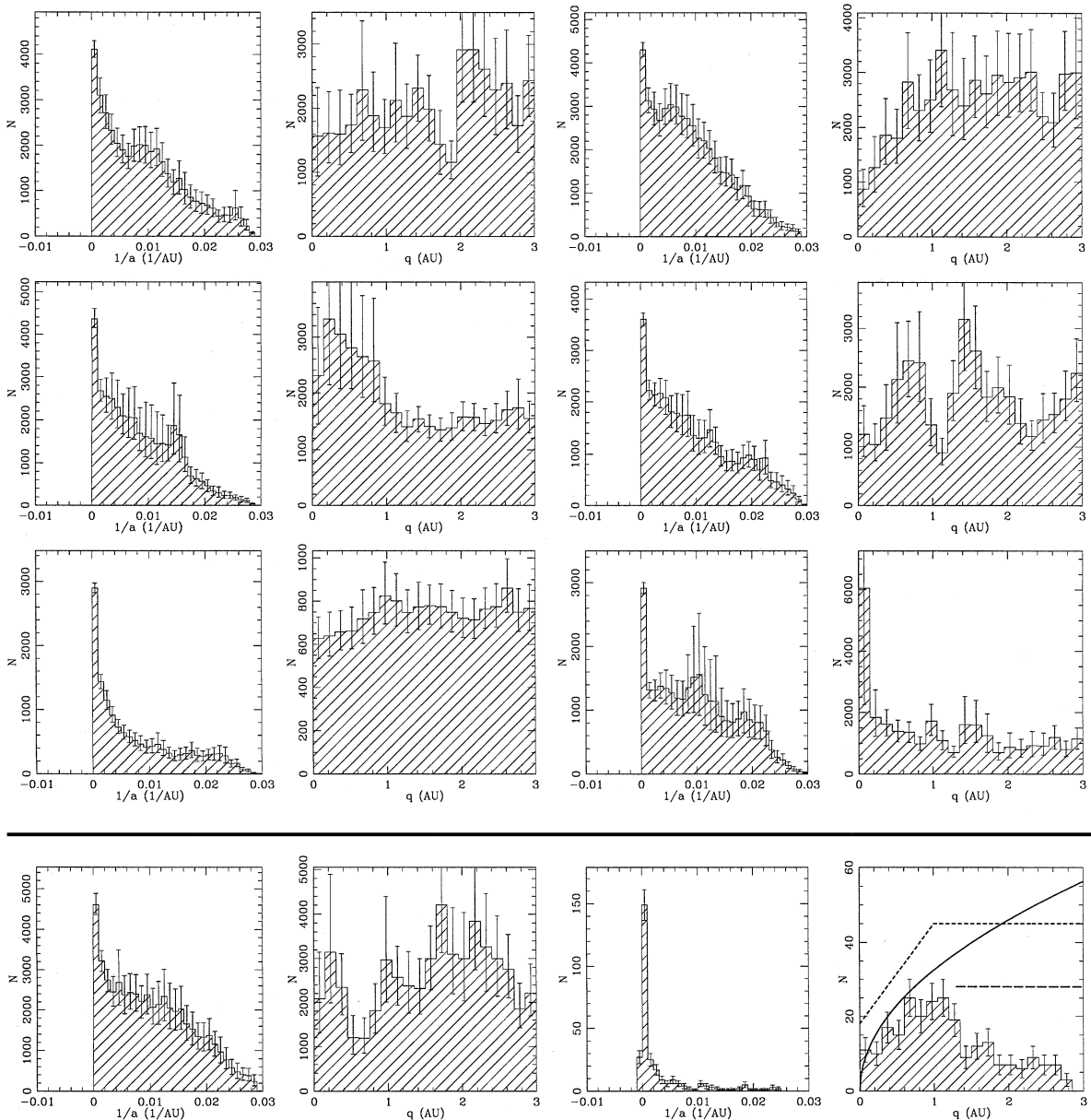
FIG. 22. Distribution of the inverse semimajor axis $1/a$ and perihelion distance q for the V_∞ comets, when the Solar System contains a massive solar companion. Left panels: companion orbital radius of 100 AU. Right panel: orbital radius 1000 AU. From the top down, the companion masses are 0.1, 1, and 10 Jupiter masses. The bottom line of panels is for comparison, and includes the standard model (left side) and the observations (right side). The observed perihelion distribution includes curves indicating the estimated intrinsic distribution (see Fig. 15 for details).

typically close to but below unity. The model does not match the observations for any value of the parameter m_v.

Figure 24 displays the behavior of the parameters X_i given a fixed fading probability λ per apparition (model [b]). Once again, the results are almost independent of NG forces and the visibility criterion, and there is no value for the parameter λ that matches the observations ($X_i = 1$).

Figure 25 shows the parameters X_i for a power-law fading function (model [c]). Although the match is not perfect, an exponent $\kappa = 0.6 \pm 0.1$ provides a much better match than

the previous two models: $X_1 = 0.72 \pm 0.09$, $X_2 = 0.96 \pm 0.26$, and $X_3 = 0.94 \pm 0.12$ when the standard NG model and discovery probability (Eq. (1)) are used. The distributions of orbital elements are shown in Fig. 26, to be compared with the observed distributions in Section 2. For $m \gg 1$, this fading law is the same as an empirical law suggested by Whipple (1962), $\phi_m \equiv \Phi_m - \Phi_{m+1} \propto m^{-\kappa-1}$; Whipple estimated $\kappa = 0.7$.

5.5.2. Other fading functions. We have also examined several two-parameter fading functions.
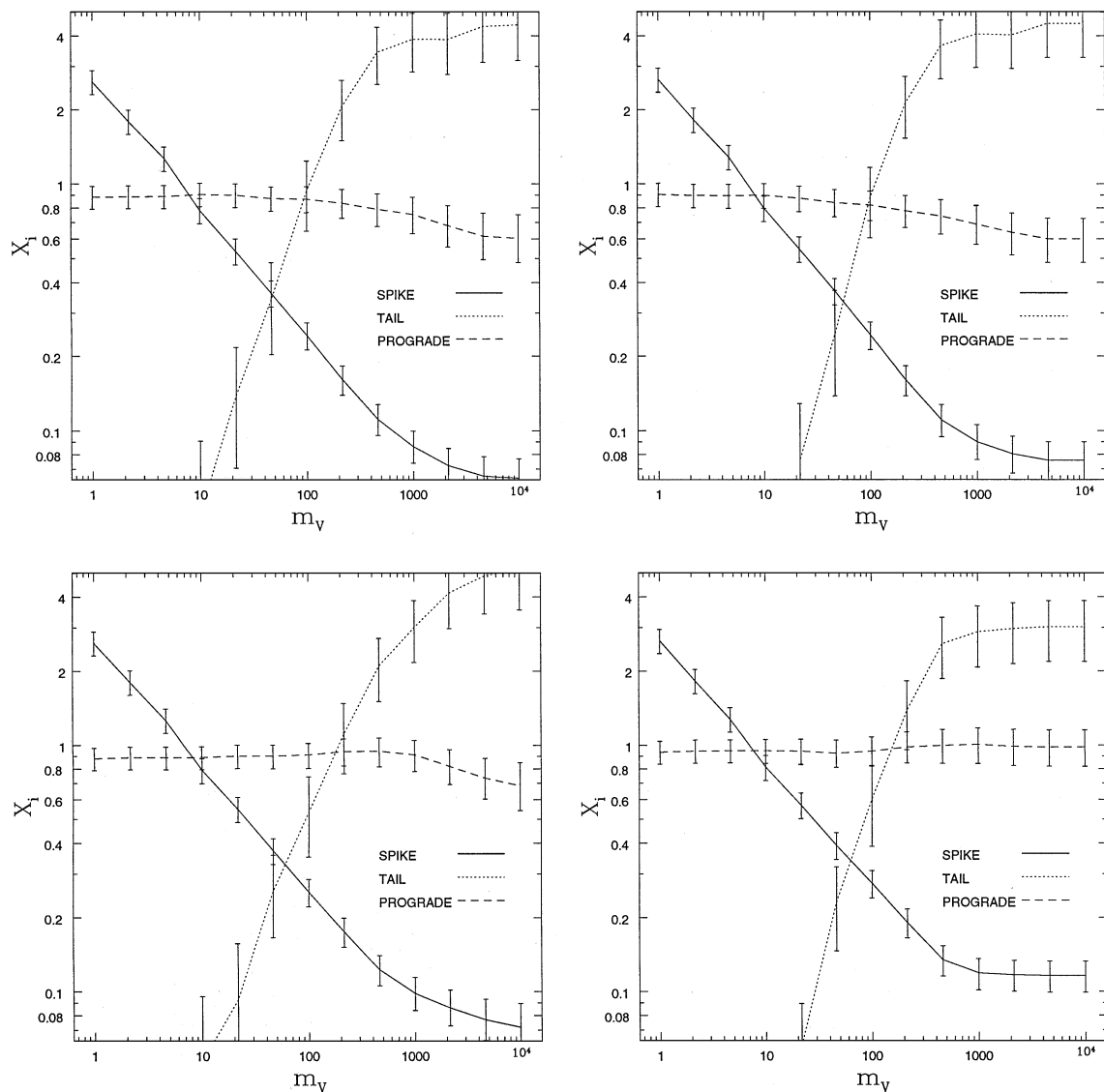
FIG. 23. The values of the parameters X_i for a fading function with a fixed lifetime of m_v apparitions (model [a], Eq. (43)). If the simulation agrees with the observations then $X_i = 1$, $i = 1, 2, 3$. The parameter X_1 is based on the fraction of LP comets in the Oort spike (solid curve); X_2 is based on the fraction of comets in the energy tail, $x > 0.0145$ AU^{-1} (dotted curve); X_3 is based on the fraction of prograde comets (dashed curve) (cf. Section 2.8). The panels on the left are based on the visibility criterion $q < 3$ AU, and those on the right are based on the visibility probability (Eq. (1)). The upper panels are based on the standard model with no NG forces, and the lower panels are based on the standard NG model.

(d) *Two populations.* Suppose that the Oort cloud contains two populations of comets, distinguished by their internal strength. The first and more fragile set is disrupted after m_v apparitions, while the more robust comets, composing a fraction f of the total, do not fade at all. Thus

$$\Phi_m = 1, \quad m \le m_v, \qquad \Phi_m = f, \quad m > m_v. \quad (46)$$

Models containing a fixed fraction of nonfading comets were proposed by Weissman (1978, 1979). The fading function with $m_v = 1$ models the case where comets fade rapidly after their first apparition, perhaps because of loss of volatiles.

(e) *Constant fading probability plus survivors.* One population has a fixed fading probability λ per apparition, while the more robust comets, composing a fraction f of the total, do not fade at all. Thus

$$\Phi_m = (1 - f)(1 - \lambda)^{m-1} + f. \quad (47)$$

(f) *Offset power law.* The fading function is chosen to be

$$\Phi_m = [(m + \beta)/(1 + \beta)]^{-\kappa}, \quad (48)$$

where β and κ are both constants. This function is similar to a power law, but drops off more slowly.
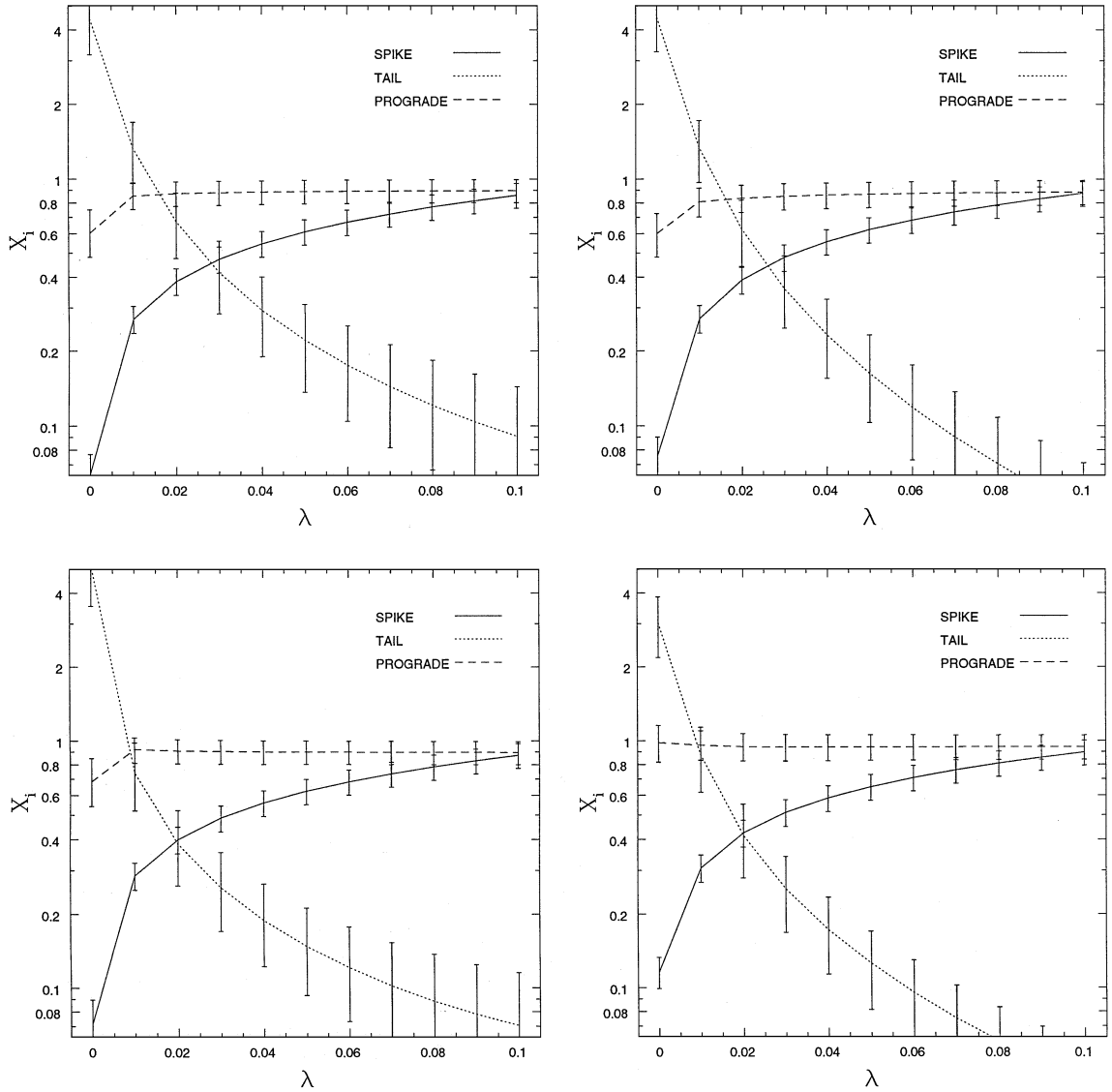
FIG. 24. The values of X_i given a fixed fading probability λ per apparition (model [b], Eq. (44)). For further details see the caption to Fig. 23.

The results of model (d) are shown in Fig. 27. In most cases the fit is worse than in the one-parameter model (a), shown by the heavy lines, because the prograde fraction described by X_3 is lower when some of the comets do not fade. The best match is for the standard NG model with visibility probability (1) (lower right panel). Here the parameters $m_v = 6$, $f = 0.04$ yield $X_1 = 0.82 \pm 0.10$, $X_2 = 0.91 \pm 0.26$, $X_3 = 0.95 \pm 0.11$, slightly better than the match for model (c). This model is reminiscent of Weissman's (1978) favored model, in which 85% of LP comets had significant fading probabilities while the remainder survived indefinitely. The best fit with $m_v = 1$, corresponding to fading after the first apparition, has $f \simeq 0.03$ and yields X_1, $X_3 \simeq 1.5$.

Model (e) is a generalization of the one-parameter model (b) but ordinarily does no better: the match to observations is usually best when the survivor fraction f is set to zero, and gets worse as f increases. Model (f) also does no better than its one-parameter

counterpart, model (c). More detailed descriptions of the models can be found in Wiegert (1996).

Finally, we examine

(g) *Other published fading functions.* In Section 3.3, we described a number of fading functions deduced in previous studies. Oort (1950) took $\psi_1 = 0.8$, $\psi_m = 0.014$ for $m > 1$; Kendall (1961) took $\psi_1 = 0.8$, $\psi_m = 0.04$ for $m > 1$; Whipple (1962) took $\phi_m \propto m^{-1.7}$; Weissman (1978) took $f = 0.15$, $\lambda = 0.1$ (cf. Eq. (47)); Everhart (1979) took $\Phi_1 = 1$, $\Phi_m = 0.2$ for $m > 1$; Bailey's (1984) fading law is described by Eq. (13); and Emel'yanenko and Bailey (1996) assume $\Phi_m = 0.3$ but add a probability $k^* = 0.0005$ that the comet is "rejuvenated." In Table 8, we have listed the values of X_i obtained for all these fading models (the results in the table are based on the model that includes the discovery probability (1) and standard NG forces; other models give very similar results). Many provide
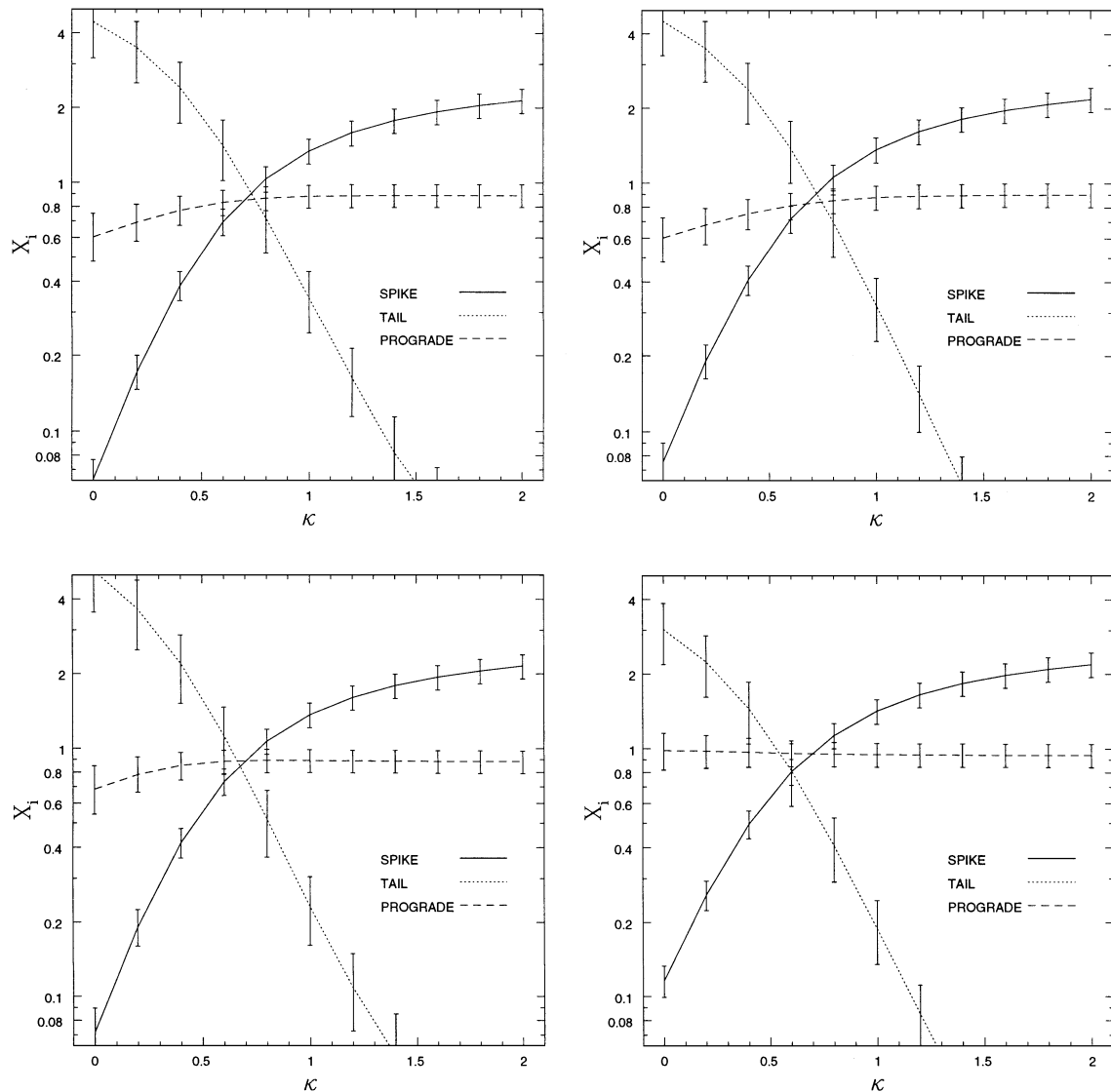
FIG. 25. The values of X_i given a power-law fading function with exponent $-\kappa$ (model [c], Eq. (45)). For further details see the caption to Fig. 23.

reasonable matches to the data but none do as well as our best fits. However, the parameters of these models were not all chosen to optimize the fit to the features of the LP comet distribution used here. The comparison is thus not entirely a fair one, but is presented for completeness.

6. SUMMARY

The LP comets provide our only probe of the properties of the Oort comet cloud. The expected distribution of their orbital elements is only weakly dependent on the properties of the Oort cloud and is straightforward—though not easy—to predict if the distribution is in a steady state. Thus a central problem in the study of comets is to compare the predicted and observed distributions of the orbital elements of the LP comets.

We have simulated the dynamical evolution of LP comets from their origin in the Oort cloud until the comets are lost or destroyed. We have integrated the comet trajectories under the influence of the Sun, the giant planets, and the Galactic tide. In some cases we have included the effects of nongravitational forces, a hypothetical circumsolar disk or solar companion, and the disruption or fading of the comet nucleus. We have not included the effects of passing stars on the Oort cloud; these add a random component to the expected distribution of LP comets which is more difficult to model but is not expected to strongly affect the distribution except during rare comet showers (cf. Section 4.1.3). Our conclusions from these simulations include the following:

The Oort cloud presently contains roughly $2 \times 10^{12}(\Phi_{\text{new}}/12 \text{ yr}^{-1})$ objects orbiting between 10,000 and 50,000 AU from the Sun (Eq. (36)), assuming that the cloud is in a steady state
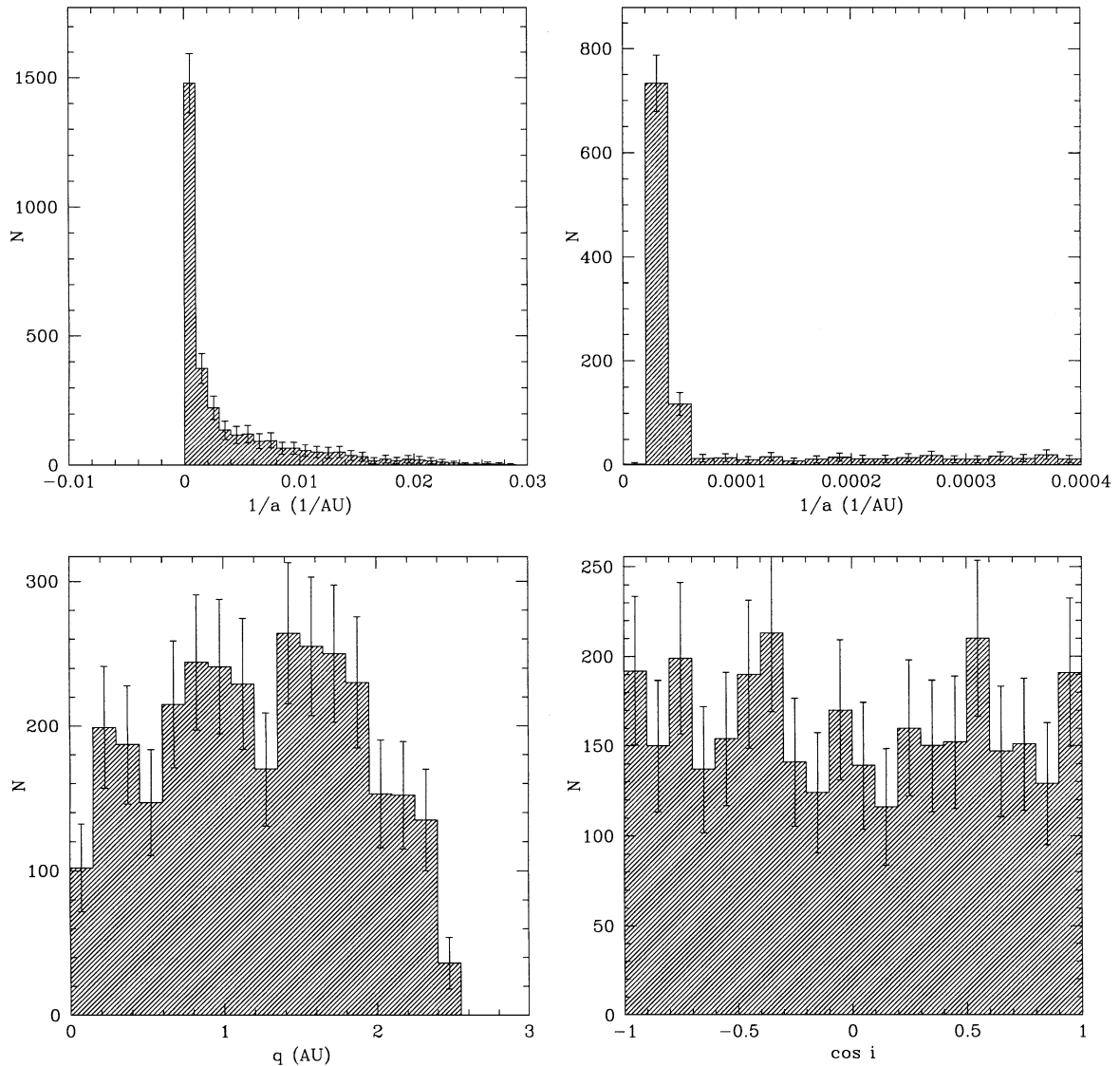
FIG. 26. The distribution of the inverse semimajor axis $1/a$, perihelion distance q, and cosine of the ecliptic inclination i for a power-law fading function with exponent $\kappa = -0.6$ (Eq. (45)). These simulations are based on the standard NG model and the visibility probability in Eq. (1).

and that the number density in the cloud is proportional to $r^{-3.5}$ (Duncan *et al.* 1987); here Φ_{new} is the observed flux of dynamically new comets with perihelion <3 AU. This estimate depends strongly on uncertain assumptions about the density and extent of the inner Oort cloud; a more reliable parameter is that the number of comets in the outer Oort cloud ($a > 20,000$ AU) is $1 \times 10^{12}(\Phi_{new}/12 \text{ yr}^{-1})$.

Over 90% of the comets in the Oort spike ($1/a < 10^{-4}$ AU^{-1}) are making their first apparition (Section 5.2), and only 2% of dynamically new comets have energies outside the spike (Section 5.1). The Oort cloud provides only about 10% of the observed SP comets, and possibly less if LP comets fade. Thus another source, such as the Kuiper belt, must provide the bulk of the SP comets. On the other hand, a significant fraction of the Halley-family comets may arise in the Oort cloud; however, biases in

and the small size of both the observed and simulated sample of Halley-family comets render this estimate very approximate.

LP comets collide with Jupiter and Saturn roughly once per 15,000 yr if $\Phi_{new} = 12$ yr^{-1} (Section 5.2.2).

This research does not explain the existence of a few comets on hyperbolic original orbits (see Fig. 1). The excess velocities are small, corresponding to roughly -10^{-4} AU^{-1} in inverse semimajor axis, but are larger than those produced by the Galactic tide ($\sim -10^{-6}$ AU^{-1}), by the model for nongravitational forces used here ($\sim -10^{-5}$ AU^{-1}) or by a circumsolar disk or solar companion small enough to be compatible with the distribution of bound orbits. Thus our results are consistent with the hypothesis of previous researchers that the hyperbolic comets are a result of small errors in their orbital determinations or unmodeled non-gravitational forces (*e.g.*, Marsden *et al.* 1973).
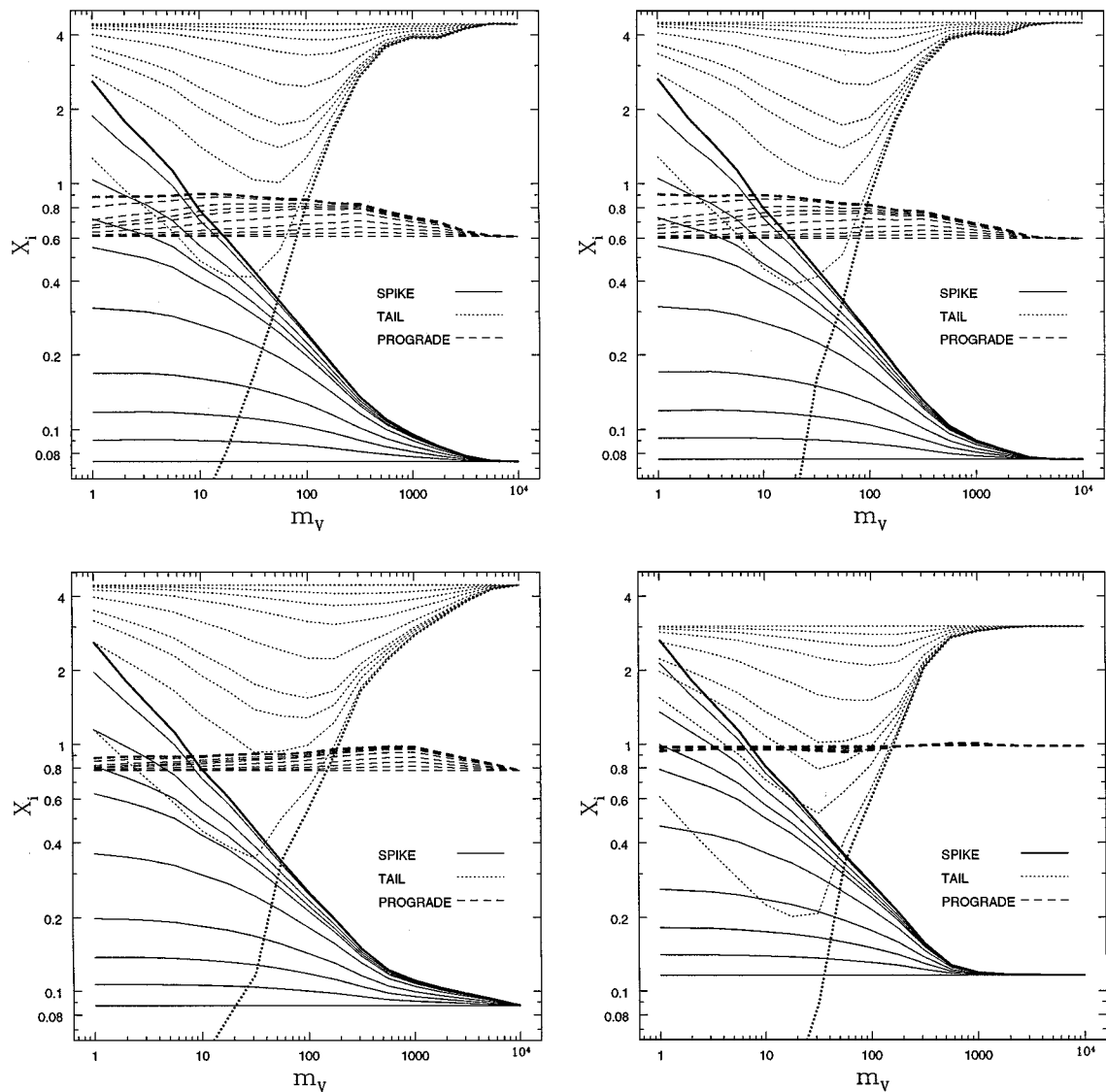
FIG. 27. The values of X_i given a two-parameter fading function in which a fraction $1 - f$ survives for m_v apparitions, while a fraction f survives forever (model [d], Eq. (46)). The fractions f for the different curves are 0, 0.01, 0.04, 0.07, 0.1, 0.2, 0.4, 0.6, 0.8, and 1, beginning with the heavy lines. For further details see the caption to Fig. 23.

Using simple models based on a one-dimensional random walk (Section 3.3), many investigators, starting with Oort (1950), have concluded that the observed energy distribution of LP comets is incompatible with the expected steady-state distribution, unless many new comets are destroyed before their second or subsequent perihelion passage. We have shown that this "fading" problem persists in a simulation that follows the comet orbits in detail.

Non-gravitational forces play a significant role in shaping the distributions of the orbital elements of the LP comets, but are too small by at least two orders of magnitude to resolve the fading problem (Section 4.2). Hypothetical additional components of the Solar System such as a massive circumsolar disk or solar companion also do not resolve the fading problem (Section 5.4).

We can match the observed distribution of orbital elements to the expected steady-state distribution with at least two fading functions: (a) a one-parameter power-law (Eq. (45)) with exponent $\kappa \simeq 0.6$ (Whipple 1962); (b) a two-population model (Eq. (46)) in which approximately 95% of comets survive for roughly six orbits and the remainder do not fade (the latter model is also roughly consistent with the observed splitting probabilities of dynamically new LP comets, approximately 0.1 per orbit; see Weissman 1980). We also note that models in which comets fade after the first perihelion passage—as might be expected if fading is due to depletion of volatiles—do not fit as well as models in which fading occurs after the first few perihelion passages. Similarly in the power-law model, the fraction of unfaded comets drops below 20% only after 15 apparitions.

TABLE 8
The values of X_i for the Preferred Fading Models of Oort 1950, Kendall 1961, Whipple 1962, Weissman 1978, Everhart 1979, Bailey 1984, and Emel'yanenko and Bailey 1996

Name	X_1	X_2	X_3
Oort	0.66 ± 0.09	1.21 ± 0.44	0.91 ± 0.13
Kendall	0.98 ± 0.12	0.59 ± 0.24	0.91 ± 0.12
Whipple	0.96 ± 0.11	0.58 ± 0.16	0.94 ± 0.11
Weissman	0.50 ± 0.07	2.07 ± 0.58	0.97 ± 0.14
Everhart	0.47 ± 0.08	2.60 ± 0.73	0.96 ± 0.15
Bailey	0.82 ± 0.11	1.68 ± 0.63	1.06 ± 0.13
Emel'yanenko	0.69 ± 0.08	0.16 ± 0.05	0.94 ± 0.11
Model (c)	0.72 ± 0.09	0.96 ± 0.26	0.94 ± 0.12
Model (d)	0.82 ± 0.10	0.91 ± 0.26	0.95 ± 0.11

Note. The final two lines are for the fading functions (c) and (d) with the best-fit parameters described in the text. The results are based on the model which includes the discovery probability (Eq. (1)) and the standard NG forces.

Although physically plausible, fading remains an *ad hoc* explanation for the distribution of LP comet orbits which has not been independently confirmed, and we should remain alert for other possible explanations.

ACKNOWLEDGMENTS

REFERENCES

Antonov, V. A., and Z. P. Todriya 1984. Systematic and random deformations of long-period comet orbits. *Sov. Astron. Lett.* **10,** 166.

Artymowicz, P. 1994. Modeling and understanding the dust around β Pictoris. In *Circumstellar Dust Disks and Planet Formation* (R. Ferlet and A. Vidal-Madjar, Eds.), pp. 47–65. Editions Frontières, Gif sur Yvette.

Backman, D. E., A. Dasgupta, and R. E. Stencel 1995. Model of a Kuiper belt small grain population and resulting far infrared emission. *Astrophys. J.* **450,** L35–38.

Bahcall, J. N. 1984. Self-consistent determinations of the total amount of matter near the Sun. *Astrophys. J.* **276,** 169–181.

Bahcall, J. N., C. Flynn, and A. Gould 1992. Local dark matter density from a carefully selected sample. *Astrophys. J.* **389,** 234–250.

Bailey, M. E. 1983. The structure and evolution of the Solar System comet cloud. *Mon. Not. R. Astron. Soc.* **204,** 603–633.

Bailey, M. E. 1984. The steady-state $1/a$ distribution and the problem of cometary fading. *Mon. Not. R. Astron. Soc.* **211,** 347–368.

Bailey, M. E., J. E. Chambers, and G. Hahn 1992. Origin of sungrazers—A frequent cometary end-state. *Astron. Astrophys.* **257,** 315–322.

Bailey, M. E., D. A. Wilkinson, and A. W. Wolfendale 1987. Can episodic comets showers explain the 30-Myr cyclicity in the terrestrial record? *Mon. Not. R. Astron. Soc.* **227,** 863–885.

Benner, L. A. M., and W. B. McKinnon 1995. On the orbital evolution and origin of Comet Shoemaker–Levy 9. *Icarus* **118,** 155–168.

Binney, J., and S. Tremaine 1987. *Galactic Dynamics.* Princeton Univ. Press, Princeton, NJ.

Bogart, R. S., and P. D. Noerdlinger 1982. On the distribution of orbits among long-period comets. *Astron. J.* **87,** 911–917.

Carusi, A., and G. B. Valsecchi 1992. Dynamics of comets. In *Chaos, Resonance and Collective Dynamical Phenomena in the Solar System* (S. Ferraz-Mello, Ed.), pp. 255–268. Kluwer Academic, Dordrecht.

Chirikov, B. V., and V. V. Vecheslavov 1989. Chaotic dynamics of Comet Halley. *Astron. Astrophys.* **221,** 146–154.

Delsemme, A. H., and D. C. Miller 1971. Physico-chemical phenomena in comets. III. The continuum of Comet Burnham (1960 II). *Planet. Space Sci.* **19,** 1229–1257.

Delsemme, A. H., and M. Patmiou 1986. Galactic tides affect the Oort cloud: An observational confirmation. In *Proc. 20th ESLAB Symposium on the Exploration of Halley's Comet*, Vol. 2, pp. 409–412. ESA Publications, Noordwijk.

Dones, L., H. F. Levison, and M. Duncan 1996. On the dynamical lifetimes of planet-crossing objects. In *Completing the Inventory of the Solar System* (T. W. Rettig and J. M. Hahn, Eds.), pp. 233–244. Astron. Soc. Pacific, San Francisco.

Drapatz, S., and H. Zinnecker 1984. The size and mass distribution of galactic molecular clouds. *Mon. Not. R. Astron. Soc.* **210,** 11–14.

Duncan, M., and H. Levison 1997. A disk of scattered icy objects and the origin of Jupiter-family comets. *Science* **276,** 1670–1672.

Duncan, M., T. Quinn, and S. Tremaine 1987. The formation and extent of the Solar System comet cloud. *Astron. J.* **94,** 1330–1338.

Efron, B. 1982. *The Jackknife, the Bootstrap and Other Resampling Plans.* Society for Industrial and Applied Mathematics, Philadelphia.

Emel'yanenko, V. V., and M. E. Bailey 1996. Dynamical evolution of comets and the problem of comet fading. *Earth Moon Planets* **72,** 35–40.

Everhart, E. 1967a. Comet discoveries and observational selection. *Astron. J.* **72,** 716–726.

Everhart, E. 1967b. Intrinsic distributions of cometary perihelia and magnitudes. *Astron. J.* **72,** 1002–1011.

Everhart, E. 1968. Change in total energy of comets passing through the Solar System. *Astron. J.* **73,** 1039–1052.

Everhart, E. 1972. The origin of short-period comets. *Astrophys. Lett.* **10,** 131–135.

Everhart, E. 1976. The evolution of comet orbits. In *The Study of Comets* (B. Donn, M. Mumma, W. Jackson, M. A'Hearn, and R. Harrington, Eds.), Vol. I, pp. 445–464. NASA, Washington, DC.

Everhart, E. 1979. The shortage of long-period comets in elliptical orbits. In *Dynamics of the Solar System* (R. L. Duncombe, Ed.), pp. 273–275. Reidel, Dordrecht.

Feller, W. 1968. *An Introduction to Probability Theory and its Applications*, 3rd ed., Vol. I. Wiley, New York.

Ferlet, R., and A. Vidal-Madjar (Eds.) 1994. *Circumstellar Dust Disks and Planet Formation*. Editions Frontières, Gif sur Yvette.

Fernández, J. A. 1981. New and evolved comets in the Solar System. *Astron. Astrophys.* **96,** 26–35.

Fernández, J. A. 1994. Dynamics of comets: Recent developments and new challenges. In *Asteroids, Comets and Meteors* (A. Milani, M. di Martino, and A. Cellino, Eds.), pp. 223–240. Kluwer, Dordrecht.

Fernández, J. A., and W. H. Ip 1987. Time-dependent injection of Oort cloud comets into earth-crossing orbits. *Icarus* **71,** 46–56.

Festou, M. C. 1986. The derivation of OH gas production rates from visual magnitudes of comets. In *Asteroids, Comets and Meteors* (C. I. Lagerkvist, B. A. Lindblad, H. Lundstedt, and H. Rickman, Eds.), Vol. II, pp. 299–303. Uppsala Univ. Press, Uppsala.

Festou, M. C., H. Rickman, and R. M. West 1993a. Comets. *Astron. Astrophys. Rev.* **4,** 363–447.

Festou, M. C., H. Rickman, and R. M. West 1993b. Comets. *Astron. Astrophys. Rev.* **5,** 37–163.

Good, J. C., M. G. Hauser, and T. N. Gauthier 1986. IRAS observation of the zodiacal background. *Adv. Space Res.* **6** (6), 83–86.

Hamid, S. E., B. G. Marsden, and F. L. Whipple 1968. Influence of a comet belt beyond Neptune on the motions of periodic comets. *Astron. J.* **73,** 727–729.

Harper, D. A., R. F. Loewenstein, and J. A. Davidson 1984. On the nature of material surrounding Vega. *Astrophys. J.* **285,** 808–812.

Heisler, J. 1990. Monte Carlo simulations of the Oort comet cloud. *Icarus* **88,** 104–121.

Heisler, J., and S. Tremaine 1986. The influence of the galactic tidal field on the Oort comet cloud. *Icarus* **65,** 13–26.

Heisler, J., S. Tremaine, and C. Alcock 1987. The frequency and intensity of comet showers from the Oort cloud. *Icarus* **70,** 269–288.

Hills, J. G. 1981. Comet showers and the steady-state infall of comets from the Oort cloud. *Astron. J.* **86,** 1733–1740.

Hogg, D. W., G. D. Quinlan, and S. Tremaine 1991. Dynamical limits on dark mass in the outer Solar System. *Astron. J.* **101,** 2274–2286.

Hut, P., and S. Tremaine 1985. Have interstellar clouds disrupted the Oort comet cloud? *Astron. J.* **90,** 1548–1557.

Hut, P., W. Alvarez, W. P. Elder, T. Hansen, E. G. Kauffman, G. Keller, E. M. Shoemaker, and P. R. Weissman 1987. Comet showers as a cause of mass extinctions. *Nature* **329,** 118–126.

Jewitt, D., J. Luu, and J. Chen 1996. The Mauna Kea–Cerro Tololo Kuiper belt and Centaur survey. *Astron. J.* **112,** 1225–1238.

Kannan, D. 1979. *An Introduction to Stochastic Processes*. North-Holland, New York.

Kendall, D. G. 1961. Some problems in the theory of comets, I and II. In *Proc. Fourth Berkeley Symposium on Mathematical Statistics and Probability* (J. Neyman, Ed.), pp. 99–147. Univ. of California Press, Berkeley.

Kerr, F. J., and D. Lynden-Bell 1986. Review of galactic constants. *Mon. Not. R. Astron. Soc.* **221,** 1023–1038.

Kresák, Ľ. 1982. Comet discoveries, statistics and observational selection. In *Comets* (L. L. Wilkening, Ed.), pp. 56–82. Univ. of Arizona Press, Tucson.

Kresák, Ľ., and E. M. Pittich 1978. The intrinsic number density of active long-period comets in the inner Solar System. *Bull. Astron. Inst. Czech.* **29,** 299–309.

Kuijken, K. 1991. Further limits on disklike dark matter from K dwarf kinematics. *Astrophys. J.* **372,** 125–131.

Kuijken, K., and G. Gilmore 1989. The mass distribution in the galactic disc. III. The local volume mass density. *Mon. Not. R. Astron. Soc.* **239,** 651–664.

Levison, H. F. 1996. Comet taxonomy. In *Completing the Inventory of the Solar System* (T. Rettig and J. Hahn, Eds.), pp. 173–191. Astron. Soc. Pacific, San Francisco.

Lüst, R. 1984. The distribution of the aphelion directions of long-period comets. *Astron. Astrophys.* **140,** 94–100.

Lyttleton, R. A., and J. M. Hammersley 1963. The loss of long period comets from the Solar System. *Mon. Not. R. Astron. Soc.* **127,** 257–272.

Malyshkin, L., and S. Tremaine 1998. The Keplerian map for the restricted three-body problem as a model of comet evolution. *Icarus*, submitted for publication.

Marsden, B. G. 1967. The Sungrazing comet group. *Astron. J.* **72,** 1170–1183.

Marsden, B. G. 1989. The Sungrazing comet group, II. *Astron. J.* **98,** 2306–2321.

Marsden, B. G., and Z. Sekanina 1973. On the distribution of "original" orbits of comets of large perihelion distance. *Astron. J.* **78,** 1118–1124.

Marsden, B. G., and G. V. Williams 1993. *Catalogue of Cometary Orbits*, 8th ed. IAU Central Bureau for Astronomical Telegrams—Minor Planet Center, Cambridge, MA.

Marsden, B. G., Z. Sekanina, and D. K. Yeomans 1973. Comets and non-gravitational forces, V. *Astron. J.* **78,** 211–225.

Marsden, B. G., Z. Sekanina, and E. Everhart 1978. New osculating orbits for 110 comets and analysis of original orbits for 200 comets. *Astron. J.* **83,** 64–71.

Matese, J. J., and P. G. Whitman 1989. The galactic disk tidal field and the nonrandom distribution of observed Oort cloud comets. *Icarus* **82,** 389–401.

Matese, J. J., P. G. Whitman, K. A. Innanen, and M. J. Valtonen 1995. Periodic modulation of the Oort cloud comet flux by the adiabatically changing galactic tide. *Icarus* **116,** 255–268.

Morris, D. E., and R. A. Muller 1986. Tidal gravitational forces: The infall of "new" comets and comet showers. *Icarus* **65,** 1–12.

Nakamura, T. 1979. On some anomalies of the distribution of orbital inclinations of original comets. *Pub. Astron. Soc. Jpn.* **31,** 815–820.

Neslusan, L. 1996. Perihelion point preferred direction of long-period comets and the north–south asymmetry of comet discoveries from the Earth's surface. *Astron. Astrophys.* **306,** 981–990.

Oja, H. 1975. Perihelion distribution of near-parabolic comets. *Astron. Astrophys.* **43,** 317–319.

Oort, J. H. 1950. The structure of the cloud of comets surrounding the Solar System, and a hypothesis concerning its origin. *Bull. Astron. Inst. Netherlands* **11,** 91–110.

Oort, J. H. 1960. Note on the determination of K_z and on the mass density near the sun. *Bull. Astron. Inst. Netherlands* **15,** 45–53.

Oort, J. H., and M. Schmidt 1951. Differences between old and new comets. *Bull. Astron. Inst. Netherlands* **11,** 259–269.

Petrosky, T. Y. 1986. Chaos and cometary clouds in the Solar System. *Phys. Lett. A* **117,** 328.

Press, W. H., S. A. Teukolsky, W. T. Vetterling, and B. P. Flannery 1992. *Numerical Recipes in C: The Art of Scientific Computing*, 2nd ed. Cambridge Univ. Press, Cambridge, UK.

Quinn, T., S. Tremaine, and M. Duncan 1990. Planetary perturbations and the origin of short-period comets. *Astrophys. J.* **355,** 667–679.

Sagdeev, R. Z., and G. M. Zaslavsky 1987. Stochasticity in the Kepler problem and a model of possible dynamic of comets in the Oort cloud. *Il Nuovo Cimento* **97B**(2), 119–130.

Sekanina, Z. 1964. Perihelion asymmetry of photometric curves of comets. *Bull. Astron. Inst. Czech.* **15,** 8–20.

Shoemaker, E. M. 1983. Asteroid and comet bombardment of the Earth. *Annu. Rev. Earth Planet. Sci.* **11,** 461–494.

Shoemaker, E. M., and R. F. Wolfe 1982. Cratering time scales for the Galilean satellites. In *Satellites of Jupiter* (D. Morrison, Ed.), pp. 277–339. Univ. of Arizona Press, Tucson.

Smith, B. A., and R. J. Terrile 1987. The Beta Pictoris disk: Recent optical observations. *Bull. Am. Astron. Soc.* **19,** 829.

Stephenson, F., K. Yau, and H. Hunger 1985. Records of Halley's comet on Babylonian tablets. *Nature* **314,** 587–592.

Thomas, F., and A. Morbidelli 1996. The Kozai resonance in the outer Solar System and the dynamics of long-period comets. *Celest. Mech. Dynam. Astron.* **64,** 209–229.

Torbett, M. V. 1986. Injection of Oort cloud comets to the inner Solar System by galactic tidal fields. *Mon. Not. R. Astron. Soc.* **223,** 885–895.

Tremaine, S. 1990. Dark matter in the Solar System. In *Baryonic Dark Matter* (D. Lynden-Bell and G. Gilmore, Eds.), pp. 37–65. Kluwer Academic, Dordrecht.

Tryor, J. G. 1957. The distribution of the directions of perihelia of long-period comets. *Mon. Not. R. Astron. Soc.* **117,** 370–379.

van Woerkom, A. J. J. 1948. On the origin of comets. *Bull. Astron. Inst. Netherlands* **10**(399), 445–472.

Weissman, P. R. 1978. *Physical and Dynamical Evolution of Long-Period Comets*. Ph.D. thesis, Univ. of California, Los Angeles.

Weissman, P. R. 1979. Physical and dynamical evolution of long-period comets. In *Dynamics of the Solar System* (R. L. Duncombe, Ed.), pp. 277–282. Reidel, Dordrecht.

Weissman, P. R. 1980. Physical loss of long-period comets. *Astron. Astrophys.* **85,** 191–196.

Weissman, P. R. 1984. The Vega particulate shell—Comets or asteroids? *Science* **224,** 987–989.

Weissman, P. R. 1985. Dynamical evolution of the Oort cloud. In *Dynamics of Comets: Their Origin and Evolution* (A. Carusi and G. B. Valsecchi, Eds.), pp. 87–96. Reidel, Dordrecht.

Weissman, P. R. 1990. The cometary impactor flux at the Earth. In *Global Catastrophes in Earth History* (V. L. Sharpton and P. D. Ward, Eds.), pp. 171–180. Geological Soc. Amer., Boulder, CO.

Weissman, P. R. 1996a. The Oort cloud. In *Completing the Inventory of the Solar System* (T. W. Rettig and J. M. Hahn, Eds.), pp. 265–288. Astron. Soc. Pacific, San Francisco.

Weissman, P. R. 1996b. Star passages through the Oort cloud. *Earth Moon Planets* **72,** 25–30.

Whipple, F. L. 1962. On the distribution of semimajor axes among comet orbits. *Astron. J.* **67,** 1–9.

Whipple, F. L. 1977. The reality of comet groups and pairs. *Icarus* **30,** 736–746.

Whipple, F. L. 1991. The forest and the trees. In *Comets in the Post-Halley Era* (R. L. Newburn *et al.*, Eds.), Vol. II, pp. 1259–1278. Kluwer, Dordrecht.

Whipple, F. L. 1992. The activities of comets related to their aging and origin. *Celest. Mech.* **54,** 1–11.

Whipple, F. L. 1994. The dilemma of the new-comet flux. *Planet. Space Sci.* **42,** 179–182.

Wiegert, P. A. 1996. *The Evolution of Long-Period Comets*. Ph.D. thesis, Univ. of Toronto, Toronto.

Wilhelm, K. 1987. Rotation and precession of Comet Halley. *Nature* **327,** 27–30.

Yabushita, S. 1979. A statistical study of the evolution of the orbits of long-period comets. *Mon. Not. R. Astron. Soc.* **187,** 445–462.

Yabushita, S. 1980. On exact solutions of diffusion equation in cometary dynamics. *Astron. Astrophys.* **85,** 77–79.

Yeomans, D. 1986a. Physical interpretations from the motions of Comets Halley and Giacobini–Zinner. In *Proc. 20th ESLAB Symposium on the Exploration of Halley's Comet* (B. Battrick, E. J. Rolfe, and R. Reinhard, Eds.), Vol. 2, pp. 419–425. ESA Publications, Noordwijk.

Yeomans, D. 1986b. The intermediate comets and nongravitational effects. *Astron. J.* **91,** 971–973.